PRIMARY RESEARCH ARTICLE

Ocean acidification causes variable trait-shifts in a coral species

Núria Teixidó[1,2] | Erik Caroselli[3] | Samir Alliouane[2] | Chiara Ceccarelli[3] | Steeve Comeau[2] | Jean-Pierre Gattuso[2,4] | Pietro Fici[3] | Fiorenza Micheli[5,6] | Alice Mirasole[1] | Stephen G. Monismith[7] | Marco Munari[1] | Stephen R. Palumbi[5] | Elizabeth Sheets[5] | Lidia Urbini[8] | Cinzia De Vittor[8] | Stefano Goffredo[3,9] | Maria Cristina Gambi[1]

[1]Stazione Zoologica Anton Dohrn, Deptartment of Integrative Marine Ecology, Ischia Marine Centre, Naples, Italy

[2]Laboratoire d'Océanographie de Villefranche, CNRS, Sorbonne Université, Villefranche-sur-mer, France

[3]Marine Science Group, Department of Biological, Geological, and Environmental Sciences, University of Bologna, Bologna, Italy

[4]Institute for Sustainable Development and International Relations, Paris, France

[5]Department of Biology, Hopkins Marine Station, Stanford University, Pacific Grove, CA, USA

[6]Stanford Center for Ocean Solutions, Pacific Grove, CA, USA

[7]Department of Civil and Environmental Engineering, Stanford University, Stanford, CA, USA

[8]National Institute of Oceanography and Applied Geophysics – OGS, Trieste, Italy

[9]Fano Marine Center, The Inter-Institute Center for Research on Marine Biodiversity, Resources and Biotechnologies, Fano, Italy

Correspondence
Núria Teixidó, Stazione Zoologica Anton Dohrn, Department of Integrative Marine Ecology, Ischia Marine Center, Ischia, Naples, Italy.
Emails: nuria.teixido@szn.it;nuria.teixido@obs-vlfr.fr

Erik Caroselli and Stefano Goffredo, Marine Science Group, Department of Biological, Geological, and Environmental Sciences, University of Bologna, Bologna, Italy.
Email: erik.caroselli@unibo.it (E.C.); s.goffredo@unibo.it (S.G.)

Abstract

High pCO$_2$ habitats and their populations provide an unparalleled opportunity to assess how species may survive under future ocean acidification conditions, and help to reveal the traits that confer tolerance. Here we utilize a unique CO$_2$ vent system to study the effects of exposure to elevated pCO2 on trait-shifts observed throughout natural populations of *Astroides calycularis*, an azooxanthellate scleractinian coral endemic to the Mediterranean. Unexpected shifts in skeletal and growth patterns were found. Colonies shifted to a skeletal phenotype characterized by encrusting morphology, smaller size, reduced coenosarc tissue, fewer polyps, and less porous and denser skeletons at low pH. Interestingly, while individual polyps calcified more and extended faster at low pH, whole colonies found at low pH site calcified and extended their skeleton at the same rate as did those at ambient pH sites. Transcriptomic data revealed strong genetic differentiation among local populations of this warm water species whose distribution range is currently expanding northward. We found excess differentiation in the CO$_2$ vent population for genes central to calcification, including genes for calcium management (calmodulin, calcium-binding proteins), pH regulation (V-type proton ATPase), and inorganic carbon regulation (carbonic anhydrase). Combined, our results demonstrate how coral populations can persist in high pCO$_2$ environments, making this system a powerful candidate for investigating acclimatization and local adaptation of organisms to global environmental change.

KEYWORDS
acclimatization/adaptation mechanisms, calcification, corals, environmental variability, natural CO$_2$ vents, ocean acidification

1 | INTRODUCTION

Understanding the effects of environmental variability and extremes on natural populations and ecosystems is a key priority as global environmental change intensifies (Bennett et al., 2019; Bozinovic et al., 2011). High local variability in physical and chemical ocean properties can create extreme climatic environments, where marine species persist under suboptimal environmental conditions such as highly variable temperatures, marginal habitats at latitudinal extremes, and acidification at CO_2 vent sites (Camp et al., 2018; Kapsenberg & Cyronak, 2019; Kroeker et al., 2019). Populations living in these unique settings experience high environmental variability and can have broad physiological tolerance to environmental stressors that would prevent survival of conspecifics living in less variable micro-environments (Bozinovic et al., 2011; Thomas et al., 2018). Two important mechanisms for intraspecific variation in tolerance to environmental variability and extremes are adjusting life traits through phenotypic plasticity and local adaptation, and these processes may interact synergistically (Hoffmann & Sgro, 2011; Savolainen et al., 2013). Phenotypic plasticity (also referred to as acclimatization) is the ability of a genotype to produce different morphological and physiological responses when exposed to different environmental conditions within an organism's lifespan, resulting in a phenotypic shift that is plastic and often reversible (Savolainen et al., 2013; Thomas et al., 2018). Adaptation is the result of natural selection on beneficial genotypes in a population where these changes are heritable and passed on to the next generation (Hoffmann & Sgro, 2011; Savolainen et al., 2013). Natural extreme environments are potential locations for climate-adapted populations where, for example, microhabitats experiencing periodic temperature extremes have shown to generate high tolerance in some reef-building corals (Palumbi et al., 2014; Thomas et al., 2018). However, there is still much to learn about the underlying mechanisms of acclimatization and adaptation to climate variability and extremes by studying populations in naturally variable environments. Such studies are critical for predicting future biological responses to rapid global environmental change.

Insights into species' tolerance to environmental change may be gained by analyzing traits that directly influence an organism's performance (Mouillot et al., 2013). Shifts in the occurrence of these traits under variable environmental conditions can reflect patterns of differential survival and growth strategies; for example, different morphological forms (e.g., massive or encrusting), longevity, size, growth rates, physical defenses, and dispersal ability (Darling et al., 2012; Teixidó et al., 2018). These traits provide relevant information about life strategies that are the result of different evolutionary and ecological processes and influence, both the fitness of individuals and the viability of natural populations (Darling et al., 2012; Mouillot et al., 2013; Teixidó et al., 2018). However, we still know comparatively little about trait-shifts within natural populations and the capacity to adapt to long-term novel environmental conditions.

Natural volcanic CO_2 vents cause local acidification of seawater and are used as a proxy to study future ocean acidification (Enochs et al., 2015; Fabricius et al., 2011; Hall-Spencer et al., 2008). Ocean acidification reflects a suite of changes in seawater carbonate chemistry due to the uptake of excess anthropogenic CO_2 by the ocean, resulting in a decline in the surface ocean pH, carbonate ion concentration, and saturation state of calcium carbonate minerals (e.g., aragonite) while increasing the partial pressure of carbon dioxide (pCO_2) and bicarbonate ion concentrations (Doney et al., 2009). Low pH levels in natural CO_2 vents represent future climatic conditions where, relative to 1870, surface pH is projected to decline by −0.14 to −0.4 pH units by 2100, under IPCC Representative Concentration Pathways (RCP) RCP 2.6 (low CO_2 emissions) and RCP 8.5 (high CO_2 emissions; Fabricius et al., 2011; Gattuso et al., 2015; Goffredo et al., 2014; Teixidó et al., 2018). Although these pH conditions can provide some insight into future acidification scenarios, they are not perfect proxies. One important assumption to consider is that variability of seawater pH increases with decreasing means at CO_2 vent systems. Although variability in pH/pCO_2 will increase with dissolved inorganic carbon due to the thermodynamics of the carbonate system in the future ocean (Takeshita et al., 2015), it is not possible to disentangle the effects of changes in the mean versus variability in this system. Thus, the conditions in the pH zones should be considered as pH regimes, with decreases in mean pH coinciding with increases in variability. Nevertheless, these high pCO_2 environments and their populations provide an unparalleled opportunity to assess how species may survive into future pH conditions and to reveal if general traits that confer tolerance can be identified.

Corals are marine organisms that are vulnerable to the impacts of climate change and ocean acidification (Brandl et al., 2019; Gattuso et al., 2015). They create habitats for many species, enhancing biodiversity, playing fundamental ecological roles, and sustaining ecosystem processes and services such as fisheries, coastal protection, and tourism (Brandl et al., 2019; Gattuso et al., 2015). Ocean acidification may pose a major threat to corals because their growth relies on the precipitation of calcium carbonate (calcification), a process that is expected to decrease as seawater acidity increases (Chan & Connolly, 2013). Studies conducted at CO_2 vent ecosystems on native corals have reported an overall decline in species abundances, decreases in calcification and skeletal density with increasing acidification (Fabricius et al., 2011; Fantazzini et al., 2015; Goffredo et al., 2014).

Here we utilize a unique CO_2 vent system to investigate the effects of exposure to elevate pCO_2 on trait-shifts on *Astroides calycularis*, an azooxanthellate scleractinian coral endemic to the Mediterranean, that naturally occurs in the acidified environment of a newly discovered CO_2 vent system in Ischia, Italy. This CO_2 vent system locally acidifies the seawater with gas comprising 92%–95% CO_2 (no sulfur, and no temperature anomaly). *A. calycularis* is a long-lived coral (large colonies may have a lifespan of several decades), considered a warm-water species with a narrow temperature tolerance confined to 14°C during winter (Bianchi, 2007; Zibrowius, 1995). *A. calycularis* has low dispersal capacities, and therefore restricted

gene flow (Casado-Amezúa et al., 2012). Because *A. calycularis* is a calcifying and long-lived species with low dispersal capacity, and found throughout the CO_2 vents, it is a great model system for investigating variation in local climate phenotypic plasticity and adaptation. Previous research on the effects of ocean acidification on *A. calycularis* has shown contrasting results: a reduction of net calcification rates was found when colonies growing in ambient pH conditions were transplanted to a vent system with pH below 7.7 (Prada et al., 2017), while no change in calcification under acidification was observed in controlled laboratory conditions (Movilla et al., 2016). We compare populations living near the vent to two reference areas outside the influence of CO_2 venting to examine the effects of low pH conditions on *A. calycularis* traits, to characterize the genetic population structure, and to identify differentiation in genes that are central to calcification. Specifically, we addressed the following questions: (a) do populations at the CO_2 vent and reference sites exhibit significant trait variation?, (b) do these nearby populations display genetic differentiation?, and (c) does the CO_2 vent population have highly divergent SNP genotypes from calcification related loci? To answer these questions, we characterized the physical and chemical parameters of the study sites and combined in situ population demographics, skeletal characteristics, computed tomography and transcriptomic approaches to assess changes in population

abundance, skeletal properties, age, and genomics of differentiation of *A. calycularis*.

2 | MATERIALS AND METHODS

2.1 | Experimental design and study sites

Here we compare natural populations of the scleractinian coral *A. calycularis* at a volcanic CO_2 vent and two nearby reference sites with ambient pH and no vent activity along the coast of Ischia, Italy (Figure 1). The CO_2 vent system is located at a 5 m depth inside a semi-submerged cave of volcanic origin named *Grotta del Mago* (Magician's Cave, 40°42′41.87″N, 13°57′51.06″E, hereafter Vent system; Figure 1). The cave (total length of 110 m) consists of a main outer chamber (10 m wide × 30 m long), connected to an inner chamber by a long narrow passage (Cinelli et al., 1977). Published studies and personal observations indicated an increase in the CO_2 vent activity over the last 50 years in the main chamber, with limited vent activity in the 1970s (Cinelli et al., 1977) and 2000s (Dappiano & Gambi, 2004) developing into intense activity from 2014 onwards. The abundance of *A. calycularis* in the cave has increased over time, with a low and patchy distribution

FIGURE 1 New CO_2 vent system and pH time series and variability. (a) Map showing the location of the study sites along the coast of Ischia Island, Italy. V refers to the CO_2 vent system named *Grotta del Mago*: A1 (Ambient 1, Punta Vico) and A2 (Ambient 2, Sant'Angelo) are off-vent reference sites with ambient pH. (b) The underwater volcanic vents occur in a semi-submerged cave at 5 m depth, release continuously gaseous emissions (92%–95% CO_2, no sulfur), and do not elevate temperature (Supporting Note 1; Figure S1; Tables S1 and S5). (c, e) Time series and (d, f) and pH_T (total scale) variability at the CO_2 vent site at 2 m (orange), 3 m (red), and 4 m (violet) depth and at reference sites at 2 m with ambient pH (blue). Dates of pH_T series: from September 8 to September 24, 2018 ($n = 1,530$ for each depth at the CO_2 vent site and $n = 1,331$ for the ambient pH site 1), and from May 30 to June 18, 2019 ($n = 1,840$ for each depth at the CO_2 vent site and $n = 1,691$ for the ambient pH site 2). Measurements were taken every 15 min using SeaFETs sensors. Photo credit: E. Ballesteros
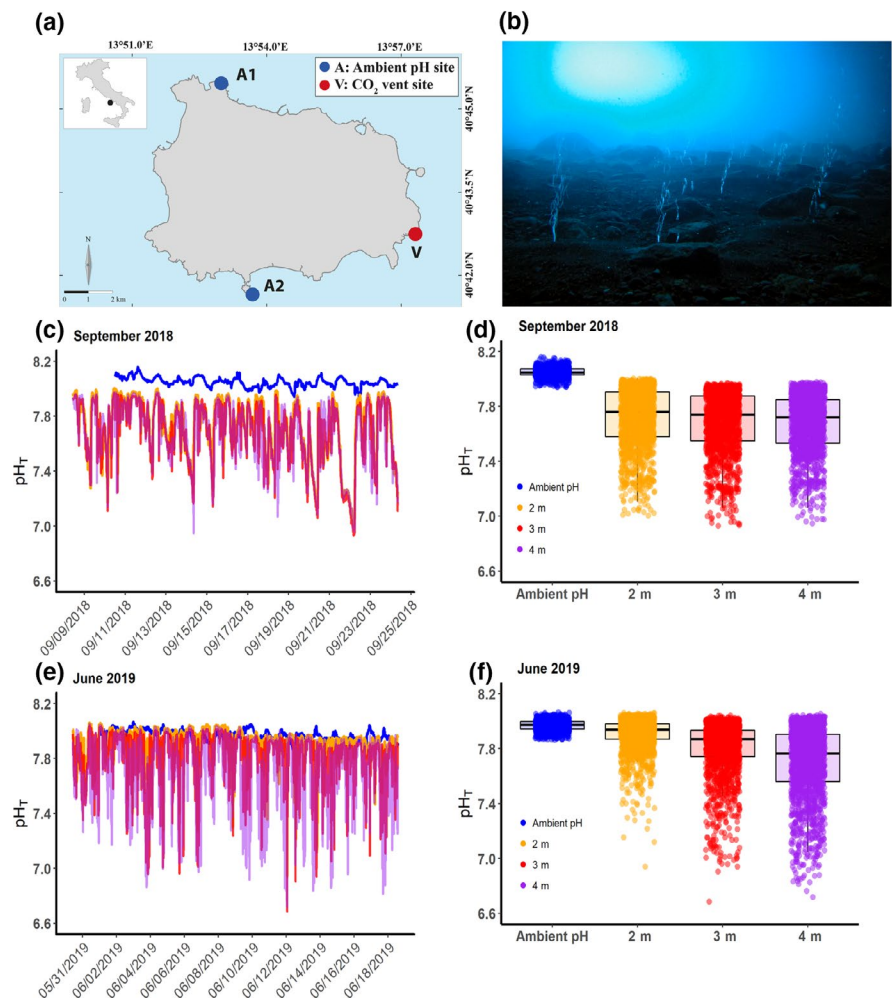
between 1 and 2 m depth in the main chamber in the 1970s (Cinelli et al., 1977) to a high and continuous distribution in the 2000s (Dappiano & Gambi, 2004). The present study was performed in the main chamber of the cave. The reference sites with ambient pH were chosen following the criteria: (a) *A. calycularis* naturally occurred there, (b) they hosted similar habitats and depths as the CO_2 vent site, and (c) and no venting activity was evident. Two reference sites were selected: Punta Vico (40°45′32.28″N, 13°52′55.38″E, another semi-submerged cave, with a main chamber 10 m wide × 30 m long, 5 m maximum depth, hereafter Ambient 1); and Sant'Angelo (40°41′33.78″N, 13°53′38.88″E, an overhang, also a natural habitat of *A. calycularis,* located on a natural arch, with an opening of 10 m wide × 10 m height, 10 m maximum depth, hereafter Ambient 2). Initial investigations of the natural systems and environmental parameters started in June 2016. These preliminary environmental data were used to plan subsequent field samplings of the carbonate chemistry associated with the CO_2 vent system and reference sites in September 2018 and June 2019.

2.2 | The coral

Astroides calycularis (Pallas, 1766) is an azooxanthellate scleractinian colonial coral endemic to the Mediterranean, characterized by the bright orange color of its coenosarc and polyps (Zibrowius, 1995). It is considered a long-lived species (e.g., large colonies may have a lifespan of several decades) and commonly found in dimly lit, shallow rocky habitats (vertical walls, cave entrances, overhangs, from the intertidal fringe to 50 m depths; Zibrowius, 1995). It can be highly abundant covering more than 90% of local reefs. It has a limited geographic distribution, with a southwestern distribution in the Mediterranean Sea (Zibrowius, 1995). This coral is considered a warm-water species with a narrow temperature tolerance confined to 14°C during the winter (Bianchi, 2007). Fossil records reveal this species lived in the northwestern Mediterranean during part of the Pleistocene, where climatic fluctuations occurred leading to a reduction of the species (Zibrowius, 1995). Interestingly, observed records north of its known distribution range in Italy and Croatia suggest that it is currently expanding northward (Bianchi, 2007). Currently, *A. calycularis* is assessed as vulnerable on the IUCN Red List due to its limited geographic distribution and the historical and current regression caused by human activities in the littoral zone. *A. calycularis* broods its larvae and has relatively low dispersal capacity (Casado-Amezúa et al., 2012).

2.3 | Gas and temperature

Gas samples were collected in 200 ml glass bottles and analyzed using gas chromatography (Agilent 7890B combined with a Micro GC analyzer-INFICON, held at a constant temperature of 80°C). The mean composition of the bubbling gas was predominantly CO_2

(92%–95%, with undetectable levels of sulfur gas <0.0002%) and did not elevate the temperature (see Supporting Note 1; Figure S1), subsequently resulting in water acidification. Vent activity was sampled by counting the number of vents in randomly placed 1 m^2 quadrats ($n = 11$) in the main chamber, with approximately 5 vents m^{-2} (mean $\pm$ SE = 4.9 $\pm$ 2.7 vents m^{-2}, min = 2 vents m^{-2}; maximum = 11 vents m^{-2}). Temperature was registered every hour by in situ temperature data loggers (Hobo TidbiT v2, Onset) in the cave and the reference areas and followed ambient seasonal fluctuations, from 14.7 to 15.2°C in winter ($n = 16,754$), and from 25.5 to 26.5°C in summer ($n = 19,011$) over a 3-year period from 2016 to 2019 at 2 m depth (Figure S1; Table S1).

2.4 | pH_T time series, pH_T variability and pH sensor calibration

SeaFET^{TM} Ocean pH sensors (Satlantic) were deployed to quantify variation in pH inside the cave at 2, 3 and 4 m depth. They were deployed in May–June (before summer) and in September (after summer) to assess whether differences in water temperature stratification could influence pH across depths. Dates of deployment were from September 8 to September 24, 2018 and from May 30 to June 18, 2019. Two sensors were deployed in the reference areas during the same period (Ambient 1 in September 2018 and Ambient 2 in June 2019). Before deployment, the SeaFETs were calibrated with ambient pH water in the aquarium facilities at the Center Villa Dohrn (Ischia, Italy; for full details of pH sensor calibration, see Supporting Methods). The mean offset between calibration samples and calibrated SeaFET pH was $\pm$0.002 units, indicating high-quality pH dataset (Figure S2).

2.5 | Carbonate chemistry and nutrients

Discrete water samples were collected using Niskin bottles at the vent and reference areas with ambient pH to measure: (a) the carbonate system parameters during the pH sensor deployment, and (b) dissolved inorganic nutrients. Salinity was measured using a CTD (CTD Sea Bird Electronics SBE 19 Plus Seacat). Samples for total alkalinity (A_T) were collected using standard operating protocols (for full details, see Supporting Methods). The HCl (0.1 M) titrant solution was calibrated against certified reference materials distributed by A.G. Dickson (CRM, Batches #153, #171, and #177). Precision of the A_T measurements of CRMs was <2 and <1 μmol/kg from nominal values for September 2018 and June 2019, respectively. A_T and pH_T were used to determine the remaining carbonate system parameters at in situ temperature and depth of each sampling period in the R package seacarb v3.2.12 (for constant details, see Supporting Methods). Dissolved inorganic nutrients (nitrite NO_2, nitrate NO_3, ammonium $NH4^+$, phosphate PO_4, and silicate $Si(OH)_4$) were determined using a colorimetric method (Supporting Methods; Table S2).

2.6 | Coral field surveys: Cover, population structure, and morphology

The *A. calycularis* cover was quantified using 24 photoquadrats (25 × 25 cm) positioned along six transects at four depths: 1, 2, 3, and 4 m in the three study sites (Vent, A1, A2). Percentage cover was analyzed with ImageJ image software (National Institutes of Health, https://imagej.net/ImageJ). Size frequency distribution was calculated at 1 and 3 m depths by counting the number of polyps of each colony and each colony was then pooled into one of five size classes (I: 1–5 polyps; II: 6–10 polyps; III: 11–15 polyps; IV: 16–20 polyps; V: >20 polyps). These size classes were selected to span the range of colony sizes encountered in the field. We also assessed necrosis as the percentage of the colony exhibiting dead tissue or denuded skeleton, from white-gray to unpigmented or denuded skeleton. Finally, visual assessments were used to classify the colonies into two morphological categories: encrusting (flat growth form) and massive (extensive vertical and lateral growth). Encrusting colonies extended laterally over the surrounding substrate with a maximum height of approximately ~3 cm, whereas massive presented a greater vertical accretion which resulted in semi-spherical shapes and colony with a minimum height of ~3 cm. This categorical criterion allowed us to obtain two simple morphological variables to capture biologically relevant axes of variation.

2.7 | Sample collection for presence of coenosarc, skeletal characteristics, and growth

In all, 66 colonies of *A. calycularis* were sampled haphazardly for coenosarc, biometric, growth, and skeletal parameters. In total, 34 colonies were collected at the vent site: 16 colonies were obtained from the vicinity of the CO_2 vents at 3 m depth (vent system deep, Vd) and 18 colonies at 1–2 m depth (vent system shallow, Vs). In total, 32 colonies were collected from areas with ambient pH conditions: 17 colonies in Punta Vico, Ambient 1, 1–2 m depth; and 15 colonies in Sant'Angelo, Ambient 2, 1–2 m depth. The 66 colonies were photographed and the percentage of coenosarc (i.e., the living tissue connecting the polyps) was determined from the edges of the polyp tissue for the whole colony using ImageJ software. We calculate the area of coenosteum (the section of the skeleton located between the polyps) and subtract the area without living tissue connecting the polyps and divide by the area of coenosteum. Then, values were pooled into 10 classes, representing every 10% interval, from 100% to 0%. Loss of coenosarc in *A. calycularis* may occur mainly by two mechanisms: (a) loss of tissue due to necrosis (when colony exhibits dead tissue, from white-gray to unpigmented or denuded skeleton) or (b) the coenosarc is already absent due to physiological and morphological characteristic of the colonies.

2.7.1 | Biometric parameters

Coral skeletons were rinsed in a solution of 10% commercial chlorine bleach for 3–4 days to dissolve polyp tissue, then they were dried at room temperature for 3 days. Colony was defined as the whole calcareous skeleton, which included the polyps (corallites) and the coenosteum. The following parameters were measured: colony length (L_c, major axis of the colony) and colony width (W_c, minor axis of the colony); number of polyps in each colony (NP_c), corallite length (L_p, maximum axis of the oral disc), and corallite width (W_p, minimum axis of the oral disc; for full details, see Supporting Methods; Figures S3 and S4; Tables S3 and S4).

2.7.2 | Growth and age estimations

The age of each corallite skeleton was determined by counting the growth bands of 49–70 randomly selected corallites per site, by means of computerized tomography (CT). Growth bands are distinguished by a high-density band in winter and a low-density band in summer in temperate corals (see Supporting Methods). The age of all collected corallites was estimated using the von Bertalanffy's length–age growth function derived from the CT growth bands analysis. Coral growth is described by three parameters: linear extension rate (linear growth), net calcification rate (net mass deposited), and bulk skeletal density (mass per volume unit; Goffredo et al., 2009). The measurement of all three components is fundamental when assessing the effect of the environment on coral growth, since none of the three parameters is a perfect predictor for the other two and each species can respond differently to environmental conditions. Then, the following three coral growth parameters were calculated for both polyp and colony levels: (a) linear extension rate; (b) net calcification rate; and (c) bulk skeletal density (see below for bulk skeletal density measurements; for full details, see Supporting Methods).

2.7.3 | Skeletal parameters

Skeletal parameters of colonies were calculated by applying the buoyant weight technique through the density determination kit of the Ohaus Explorer Pro balance (±0.0001 g; for further details, see Supporting Methods). This method is based on the Archimedes principle applied to a specimen after full saturation with the same fluid in which it was submerged. The measurements required to calculate the skeletal parameters were as follows: density of the fluid medium (ρ); dry mass (DW); buoyant weight of the skeleton (BW = weight of the skeleton minus weight of the water displaced by it); and SW (saturated weight of the coral = weight of the skeleton plus weight of the water enclosed in its volume). Measurements were repeated three times to get an average for BW and SW. Based on these measurements, the following parameters were calculated: V_{MATRIX} (matrix volume = volume of the skeleton, excluding the volume of its pores); V_{PORES} (pore volume = volume of the pores in the skeleton); and V_{TOT} (bulk volume = total volume of the skeleton including its pores). Finally, the skeletal parameters of colonies were calculated: the micro-density (ratio of DW to V_{MATRIX}); the bulk density (ratio DW to V_{TOT}); and the porosity (ratio V_{PORES} to V_{TOT}).

2.8 | Sample collection for genetics and transcriptome assembly

Astroides calycularis colonies were haphazardly collected between 1 and 2 m depth to compare gene flow among populations at the study sites. In all, 19 colonies from the Vent, 14 colonies from Ambient 1, and 8 colonies from Ambient 2 were sampled for genetic analysis. RNA was extracted from a single polyp of each colony using a RNeasy kit (Qiagen Inc.) according to the manufacturer's instructions (for full details, see Supporting Methods). Approximately 1 µg of RNA was used to construct a cDNA library for each sample using the Illumina TruSeq RNA v2 Kit (Illumina; see Supporting Methods).

Libraries were sent to the Genomics Core Facility of the Health Sciences Cores at the University of Utah (Salt Lake City, UT, USA) and samples were quantified using a Bioanalyzer (Agilent; see Supporting Methods). We assembled the first de novo transcriptome of *A. calycularis* with samples collected from Ischia. The following programs and scripts were run on Stanford University's Sherlock cluster and all scripts used in this pipeline (https://github.com/bethsheets/Astroides_transcriptomics) along with a general guide are available on GitHub (https://doi.org/10.5281/zenodo.2580291). Four population-specific de novo assemblies were generated using three individuals per population for each population in the program Trinity-2.8.4 (see Supporting Methods). Prior trials mapping to available corallimorpharian genomes produced incomplete assemblies. Therefore, assembled contigs were validated to be included in the assembly by filtering for only metazoan matches found in the combined UniProt's Swiss-Prot and TrEMBL databases using BLASTX in the BLAST+ toolkit (see Supporting Methods). Matches were considered significant at values of $\leq 1 \times 10^{-3}$ and the top hit for each contig was kept for assembly filtering and annotation. Transcriptome completeness was assessed using BUSCO v3 (see Supporting Methods) against the metazoan (obd9) set. BUSCO analyses revealed that the final combined transcriptome was 97% complete (949 complete BUSCOs out of 978 searched: 366 complete single-copy, 583 complete and duplicated; 12 fragmented, and 17 missing). For the 41 individuals used for population analyses, the average overall mapping rates for each population were as follows: Vent-Grotta Mago 79% (range: 71.91–85.28), Ambient 1—Punta Vico 80% (range: 65–84.74), and Ambient 2—Sant'Angelo 80.26% (range: 71.91–85.28). After filtering, we detected 46,784 biallelic SNPs among the vent and two ambient populations.

2.8.1 | Mapping and SNP detection

For all 41 samples, raw paired- and single-end sequence files were mapped to the de novo assembly using HISAT2 (see Supporting Methods) with the very sensitive setting. Duplicate reads due to PCR were removed with Picard tools (http://broadinstitute.github.io/picard/) MarkDuplicates using the lenient validation stringency.

Overall mapping rates were compared among populations to assess whether certain populations were preferentially mapping to the de novo assembly. Transcriptome-derived single nucleotide polymorphisms (SNPs) were called on all individuals using SAMtools mpileup and BCFtools (for filter settings, see Supporting Methods).

2.8.2 | Identifying SNP candidates for environmental selection in high CO_2 conditions and enrichment analysis

We identified potential outlier SNPs related to the CO_2 vent location. We calculated pairwise F_{ST} estimates (Vent–Ambient 1, Vent–Ambient 2, Ambient 1–Ambient 2) per locus using the basic stats function with HIERFSTAT package in R (see Section 2.9). We used these estimates to compare the genetic distance for each SNP between the three populations $[F_{ST}(\text{Vent–A1}) + F_{ST}(\text{Vent–A2})]/F_{ST}(\text{A1–A2})]$. To identify potential outlier SNPs related to the CO_2 vent location, we compared the genetic distance for each SNP for the population comparisons including Grotta Mago to the genetic distance between the ambient populations A1 and A2 $[F_{ST}(\text{Vent–A1}) + F_{ST}(\text{Vent–A2})]/F_{ST}(\text{A1–A2})]$. SNPs with values over 2 showed an excess of genetic differentiation in the CO_2 Vent compared to the other ambient pH populations. Using the transcriptome assembly annotations, we searched for enrichment patterns in the contigs holding these candidate SNPs using their UniProt identifiers (https://www.uniprot.org/) in a Gene Ontology (GO) search (http://geneontology.org/).

2.9 | Statistical analyses and data visualization

2.9.1 | Environmental data analyses

Temperature, pH_T, SeaFET sensor calibration, carbonate chemistry, and figures were performed using the R packages: seacarb v3.2.12 and ggplot2 v3.1.1 (see Supporting Methods for R package references). Carbonate system parameter figures in the vent system were created with Ocean Data View software (version 5.1.2, http://odv.awi.de).

2.9.2 | Biological surveys

A linear mixed model was used to test for differences in % cover (logit transformation) as a function of site (fixed factor, three levels), depth (fixed factor, four levels), and quadrat as a random effect. Chi-square contingency tables were used to compare the size frequency distributions among sites, as well as the frequency of encrusting and massive forms. Kolmogorov–Smirnov two-sample tests were used to determine whether there were significant differences in necrosis between the CO_2 vent and ambient pH sites. These analyses were computed using lme4 v1.1.21 package implemented in R.

2.9.3 | Skeletal characteristics and growth

Relationships between biometrical and skeletal parameters were calculated using the power function model. Pearson's correlation coefficients were calculated for the relationships among biometric and skeletal parameters at both colony and polyp levels. Spearman's rank correlation coefficient was used to calculate the significance of the correlations between colony biometric and skeletal parameters and pH_T. ANOVA was used to test % cenosarc (with arcsin transformation), mean mass, polyp number, bulk density, linear extension rate, calcification rate, and porosity of the colonies and mean length of corallites among sites. We used the non-parametric Kruskal–Wallis test for differences in means for data that did not meet the assumption for normality and equal variance. Kruskal–Wallis tests were applied to mean area, length, width, micro-density of colonies, corallite mean age, polyp linear extension rate, net calcification rate, and length of central and all corallites. These analyses were computed using IBM SPSS Statistics 12.0 (IBM Corporation). The Von Bertalanffy growth model and confidence intervals (CI) were estimated through a regression analysis by least squares procedure using raw data of corallite length and age (measured by computerized tomography; see Supporting Methods). These analyses were carried out in the software MATLAB R2012a (MathWorks).

2.9.4 | Population genetics

Population genetic analyses of SNPs, Weir and Cockerham's pairwise F_{ST} estimates among populations, and the heatmap of divergent SNP genotypes were conducted in the R-based program HIERFSTAT v4.22 and ComplexHeatmap v2.4.2, respectively.

3 | RESULTS

3.1 | Carbonate chemistry associated with the CO_2 vent system in the *Grotta del Mago* cave

The CO_2 vent system occurs at a 5 m depth inside the main chamber of the cave *Grotta del Mago* with approximately 5 vents m^{-2} (Figure 1) and do not elevate temperature (Table 1; Figure S1; Table S1). The carbonate chemistry derived from discrete water samples and in situ monitoring of seawater pH_T (pH on the total scale) delineated a pH_T gradient from 4 to 2 m depth caused by the distance from the bubbling of CO_2 gas from the seafloor (92%–95% CO_2, with undetectable levels of sulfur gas <0.0002%, see Supporting Note 1; Figure 1; Table 1). pH sensors revealed reductions in mean pH_T at each depth associated with increased temporal variability in pH_T (Figure 1; Table 1; Figure S5; Table S5). Mean pH_T were as follows: 7.65–7.88 at 2 m, 7.62–7.74 at 3 m, and 7.60–7.60 at 4 m, respectively (see Table 1 and Table S5 for detailed pH statistics). At 2 m depth, 14% and 56% of the pH_T measurements were below 7.8 (projected average global sea surface pH value for the year 2100 with

the high emission scenarios RCP8.5; Gattuso et al., 2015) in June and September, respectively (Table S5). The percentage rose to 34% and 61% at 3 m depth, and 55% and 66% at 4 m depth, in June and September, respectively (Table S5). This pattern of depth-dependent low pH_T was also manifested as extreme pH events (defined as the pH value of 0.4 units less than the mean pH for each depth) that increased in number and duration with depth (Table S6). Mean pH_T and variability were influenced by temperature stratification in June and September (Figure 1; Figures S5 and S6). This is because during periods of stratification, and hence reduced vertical mixing (Turner, 1973), the input of CO_2 is likely to be primarily confined to the lower part of the water column, leading to lower pH values near bed than when the water column is well mixed. The mean temperature difference between 2 and 4 m in June was 0.25°C, whereas the mean temperature difference was only 0.02°C in September (Figure S6). In September, reductions in seawater pH_T were driven by increased dissolved inorganic carbon concentrations (C_T) and higher pCO_2 concentrations at relatively constant total alkalinities (A_T) and temperatures across depths (Table 1; Figure S5). Mean pCO_2 ranged from 2,905 ± 1,664 µatm at 2 m, to 3,146 ± 1,928 µatm at 3 m, to 3,192 ± 1,806 µatm at 4 m depth, and aragonite saturation state (Ωa) ranged from 1.10 ± 0.4 at 2 m, to 1.05 ± 0.4 at 3 m, and to 1.02 ± 0.4 at 4 m depth (Table 1). In contrast, in June, the vent site was characterized by an increase in temperature along the water column (from ~18.5 to ~25°C), which created greater difference across the three depths in terms of pH_T and associated carbonate chemistry parameters, particularly for the pCO_2 concentrations (from 1,531 ± 627 µatm at 2 m, to 2,082 ± 1,502 µatm at 3 m, and 2,812 ± 2,310 µatm at 4 m depth) and Ωa (from 1.44 ± 0.27 at 2 m, to 1.23 ± 0.35 at 3 m, to 1.05 ± 0.42 at 4 m depth; Table 1, Figure S5). At the two ambient pH sites, the mean pH_T ranged from 7.97 to 8.05 units, pCO_2 from 322 ± 34 to 586 ± 76 µatm, and Ωa from 3.54 ± 0.23 to 3.86 ± 0.23 (Table 1).

3.2 | Cover, population structure, and morphology of *A. calycularis*

The CO_2 vent population was characterized by small colonies (90% colonies had up to 10 polyps) and no large colonies of more than 20 polyps (class V) with massive morphology were found (Figure 2; Figure S7). Larger colonies (i.e., >16 polyps, size classes IV and V) were only found in the two reference areas (percentage of larger size classes ranged from 13% in A1 to 16% in A2), which differed significantly among the CO_2 vent site ($\chi^2 = 91.9$, $df = 8$, $p < .0001$). Additionally, necrosis was significantly higher at the CO_2 vent site ($13 ± 4$%) than the reference areas (both <0.5%, $D = 0.56$, $p < .0001$). *A. calycularis*' cover at the CO_2 vent site decreased from 50% at 1 m depth, to 30% at 2 m, 9% at 3 m, and 1% at 4 m depth, as seawater pH_T also declined (Figure S7). This decline in coral cover was also observed in Ambient 1 (also a cave, from 69% at 1 m to 14% at 3 m) but not in Ambient 2 (overhang, from 72% at 1 m to 62% at 3 m; $F = 14.1$, $df = 11,55$; $p < .001$; Figure S7).

TABLE 1 Measured and estimated seawater physiochemical parameters at the CO_2 vent site and reference areas with ambient pH for salinity (S), temperature (T), total alkalinity (A_T), dissolved inorganic carbon (C_T), pH_T, pCO_2, calcite (Ωc), and aragonite(Ωa) saturation. Values are means ± SD with 25th and 75th percentiles. Calculated concentrations of C_T, pCO_2, Ωc, and Ωa are shown. 1: Parameters measured from discrete water samples; 2: Parameters measured with in situ sensors. For detailed SeaFET pH sensor statistics and the carbonate system parameters, see Figure S5 and Table S5, respectively

Month (year)	Vent site (GM)			A1-PV	A2-SA
	2 m	3 m	4 m	2 m	2 m
September (2018)					
S	$37.3^{[1]} \pm 0.2$ (37.2, 37.5), n = 9	$37.3^{[1]} \pm 0.2$ (37.2, 37.5), n = 9	$37.3^{[1]} \pm 0.2$ (37.2, 37.5), n = 9	$37.3^{[1]} \pm 0$ (37.3, 37.3), n = 5	$37.4^{[1]} \pm 0$ (37.4, 37.4), n = 3
T (°C)	$25.9^{[2]} \pm 0.2$ (25.8, 26.0), n = 1,530	$26.0^{[2]} \pm 0.2$ (25.8, 26.0), n = 1,530	$26.0^{[2]} \pm 0.2$ (25.9, 26.1), n = 1,530	$17.3^{[2]} \pm 0.4$ (17.0, 17.6), n = 1,331[2]	$25.9^{[2]} \pm 0.2$ (59.9, 26.1), n = 408
A_T (µmol/kg)	$2,564^{[1]} \pm 7$ (2,561, 2,566), n = 9	$2,562^{[1]} \pm 8$ (2,557, 2,565), n = 9	$2,562^{[1]} \pm 8$ (2,556, 2,566), n = 9	$2,618^{[1]} \pm 15$ (2,607, 2,633), n = 5	$2,610^{[1]} \pm 1$ (2,609, 2,611), n = 3
C_T (µmol/kg)	$2,542 \pm 79$ (2,477, 2,585), n = 1,530	$2,552 \pm 84$ (2,485, 2,593), n = 1,530	$2,555 \pm 80$ (2,495, 2,598), n = 1,530	$2,262 \pm 24$ (2,246, 2,276), n = 1,331	$2,275 \pm 1$ (2,275, 2,276), n = 3
pH_T	$7.65^{[2]}$ (7.58, 7.90), n = 1,530	$7.62^{[2]}$ (7.55, 7.87), n = 1,530	$7.60^{[2]}$ (7.53, 7.85), n = 1,530	$8.05^{[2]}$ (8.03, 8.07), n = 1,331	$8.02^{[1]}$ (8.02, 8.03), n = 3
pCO_2 (µatm)	$2,905 \pm 1,664$ (1,724, 3,438), n = 1,530	$3,146 \pm 1,928$ (1,837, 3,668), n = 1,530	$3,192 \pm 1,806$ (1,958, 3,799), n = 1,530	322 ± 34 (298, 341), n = 1,331	375 ± 1 (374, 375), n = 3
Ωc	1.68 ± 0.59 (1.21, 2.21), n = 1,530	1.58 ± 0.56 (1.14, 2.09), n = 1,530	1.54 ± 0.54 (1.10, 1.98), n = 1,530	5.96 ± 0.36 (5.74, 6.21), n = 1,331	5.70 ± 0.01 (5.69, 5.70), n = 3
Ωa	1.11 ± 0.39 (0.80, 1.47), n = 1,530	1.05 ± 0.37 (0.75, 1.39), n = 1,530	1.02 ± 0.36 (0.73, 1.32), n = 1,530	3.86 ± 0.23 (3.72, 4.02), n = 1,331	3.71 ± 0.01 (3.70, 3.71), n = 3
June 2019					
S	$37.8^{[1]} \pm 0$ (37.8, 37.8), n = 7	$37.8^{[1]} \pm 0$ (37.8, 37.8), n = 7	$37.8^{[1]} \pm 0$ (37.8, 37.8), n = 7	$38.0^{[1]} \pm 0$ (38.0, 38.0), n = 3	$37.9^{[1]} \pm 0$ (37.9, 37.9), n = 7
T (°C)	$21.9^{[2]} \pm 2.1$ (19.9, 24.1), n = 1,840	$21.8^{[2]} \pm 2.1$ (19.8, 23.8), n = 1,840[2]	$21.7^{[2]} \pm 2.0$ (19.6, 23.4), n = 1,840[2]	$26.2^{[2]} \pm 0.2$ (26.1, 26.3), n = 408	$26.2^{[2]} \pm 1.1$ (25.8, 27.0), n = 1,691[2]
A_T (µmol/kg)	$2,539^{[1]} \pm 22$ (2,593, 2,552), n = 7	$2,541^{[1]} \pm 20$ (2,532, 2,550), n = 7	$2,551^{[1]} \pm 22$ (2,538, 2,568), n = 7	$2,630^{[1]} \pm 1$ (2,630.1, 2,630.9), n = 3	$2,642^{[1]} \pm 17$ (2,629, 2,659), n = 7
C_T (µmol/kg)	$2,450 \pm 42$ (2,424, 2,464), n = 1,840	$2,489 \pm 75$ (2,443, 2,509), n = 1,840	$2,535 \pm 104$ (2,461, 2,574), n = 1,840	$2,336 \pm 3$ (2,320, 2,353), n = 3	$2,336 \pm 23$ (2,320, 2,353), n = 1,691
pH_T	$7.88^{[2]}$ (7.86, 7.98), n = 1,840	$7.74^{[2]}$ (7.74, 7.93), n = 1,840	$7.60^{[2]}$ (7.56, 7.90), n = 1,840	$8.04^{[1]}$ (8.04, 8.04), n = 3	$7.97^{[2]}$ (7.94, 7.99), n = 1,691
pCO_2 (µatm)	$1,531 \pm 627$ (1,167, 1,653), n = 1,840	$2,082 \pm 1,502$ (1,352, 2,127), n = 1,840	$2,812 \pm 2,310$ (1,495, 3,090), n = 1,840	372 ± 1 (372, 373), n = 3	586 ± 76 (532, 635), n = 1,691
Ωc	2.20 ± 0.41 (2.01, 2.46), n = 1,840	1.87 ± 0.54 (1.57, 2.26), n = 1,840	1.60 ± 0.65 (1.10, 2.14), n = 1,840	5.92 ± 0.01 (5.92, 5.93), n = 3	5.34 ± 0.35 (5.08, 5.58), n = 1,691
Ωa	1.44 ± 0.27 (1.32, 1.61), n = 1,840	1.23 ± 0.35 (1.03, 1.48), n = 1,840	1.05 ± 0.42 (0.72, 1.40), n = 1,840	3.89 ± 0.01 (3.86, 3.87), n = 3	3.54 ± 0.23 (3.38, 3.71), n = 1,691

FIGURE 2 (a) Photographs showing colonies sampled for skeletal characteristics and growth of the CO_2 vent system and off-vent reference sites with ambient pH. Vent system deep (3 m depth); Vent system shallow (1–2 m depth), Ambient 1 = Punta Vico (1–2 m depth); Ambient 2 = Sant'Angelo (1–2 m depth). Colonies in the vent system exhibited encrusting form (flat growth form), whereas colonies in Ambient pH sites were a mixture of massive (extensive vertical and lateral growth) and encrusting forms (see also Figure S7). (b) % Coenosarc (the living tissue connecting the polyps) of colonies among the study sites. Number of colonies = 66
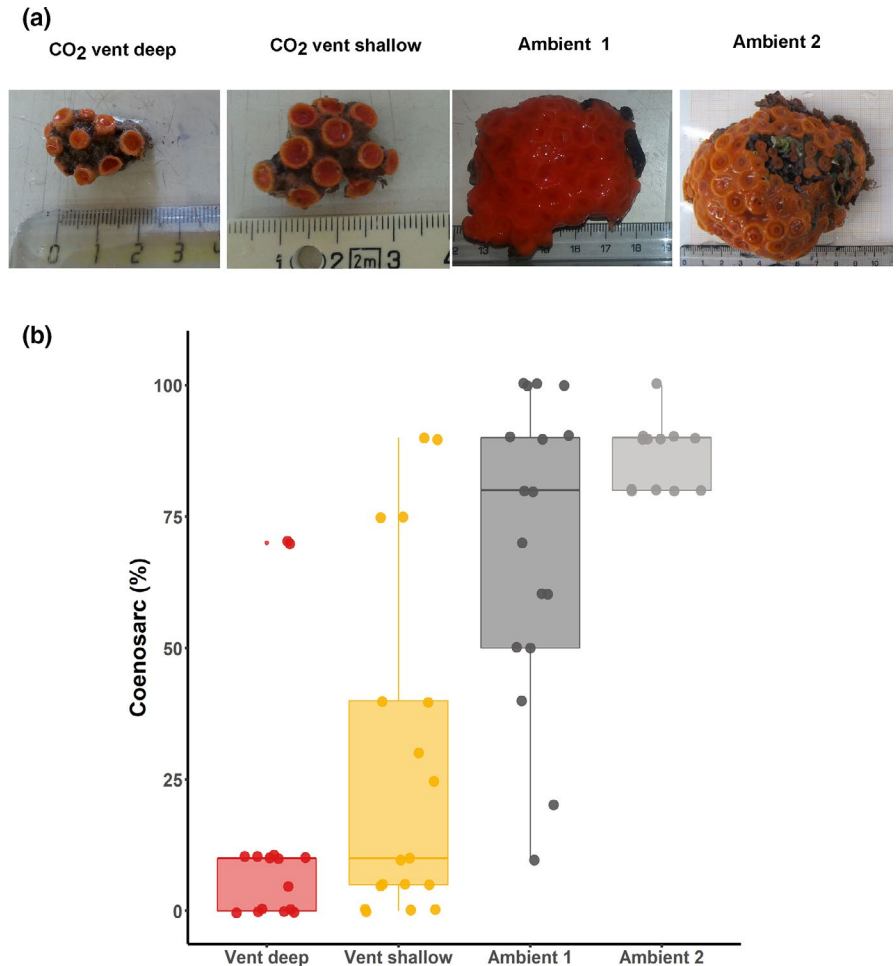
3.3 | Coenosarc, skeletal parameters, and growth

Percentage of coenosarc (the living tissue connecting the polyps) significantly decreased between ambient pH sites (87% and 70%) and the CO_2 vent (28% and 14%; Figure 2, $p < .0001$). Mean colony area decreased by ~80% to 71% and mean polyp number by ~27% to 18% at the Vent deep compared to ambient pH sites ($p < .001$; Figure 3a). The skeletal parameters that characterize the architecture of colonies showed different patterns in relation to pH (Figure 3; Figures S8 and S9). Bulk density (ratio dry mass to bulk volume) and micro-density (ratio of dry mass to matrix volume) increased at low pH, while porosity (ratio pore volume to bulk volume; see Section 2) decreased at low pH ($p < .001$; Figure 3). Colonies at the CO_2 vent deep presented higher bulk density (~ +27%) and micro-density (~ +7%) and lower porosity (~ −28%) compared to colonies from the ambient pH sites ($p < .001$; Figure 3; Figure S9).

Growth parameters of *A. calycularis* differed significantly between the CO_2 vent site and ambient pH sites (Figures 3b and 4; Figure S10; Table S7). Mean polyp growth rate decreased exponentially with age at all sites (Figure S10). Young individuals (1–3 years old) grew relatively rapidly (>2 mm/year), but, as they aged, their skeletal growth rate decreased (<1.3 mm/year at 8–10 years old; Figure 4a; Tables S7 and S8). A trend toward higher linear extension

and net calcification rate was observed at low pH at the polyp level (Figure 3b; Table S7). Polyp net calcification rate ranged from 3.95 mg mm^{-2} year^{-1} at Vent deep, to 3.04 mg mm^{-2} year^{-1} at Vent shallow, to 2.39 mg mm^{-2} year^{-1} and 2.06 mg mm^{-2} year^{-1} at ambient pH sites (Table S7). This indicates that net calcification rates increased approximately by 48%–93% from the more acidified (Vent deep) to the less acidified (Vent shallow) to the non-acidified (ambient pH) locations at polyp level. Linear extension and net calcification rates at colony level were homogeneous in ambient pH and acidified conditions (Figure 3b; Table S7).

3.4 | Transcriptome assembly and population genomics

The *A. calycularis* transcriptome composed of 12 colonies contained 113,351 contigs with an N50 of 2,285 (range 501–38,179). Based on 46,784 SNPs in 41 individuals, PCA analysis revealed strong clustering by population (Figure 5). The vent population in Grotta Mago was most distinct along PCA axis 1, but overlapped with Ambient 1 (PV) along axis 2. Pairwise F_{ST} measurements also support strong population structure within each of the three locations: CO_2 vent (Grotta Mago)–Ambient 1 (Punta Vico) = 0.034, CO_2 vent (Grotta
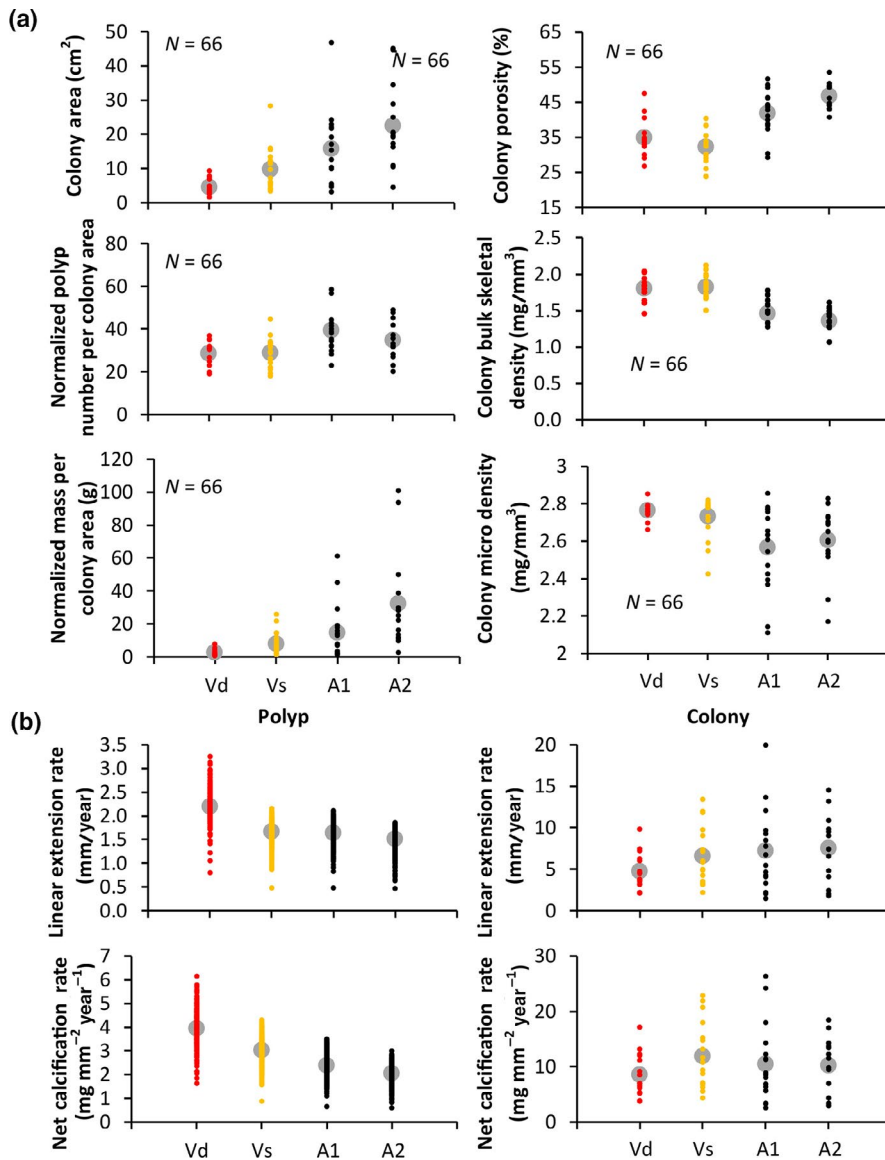
FIGURE 3 Skeletal and growth parameters measured in *Astroides calycularis*. (a) Skeletal parameters of colonies and (b) growth parameters at polyp and colony levels at the CO$_2$ vent site (Vd and Vs) and ambient pH conditions (A1 and A2), respectively. Colony mass and polyp number were normalized to colony area. Gray circles in the plot represent the mean. A1 = Ambient 1, number of colonies = 17; A2 = Ambient 2, number of colonies = 15; Vd = Vent system deep, number of colonies = 16; Vs = Vent system shallow, number of colonies = 18. Total number of colonies analyzed = 66

Mago)–Ambient 2 (Sant'Angelo) = 0.026, Ambient 1 (Punta Vico)–Ambient 2 (Sant'Angelo) = 0.024. SNPs with values over 2 show an excess of genetic differentiation in GM compared to the other populations. There were 334 loci with an excess F_{ST} ratio of 10 or more, out of 2,246 loci in our dataset with known molecular function. An analysis of the 402 unique molecular function gene ontology (GO) terms associated with these loci showed there to be three significant enrichment classes (Table S9): calcium ion binding (12 loci, $p_{adj} = 7 \times 10^{-23}$), catalytic activity (4 loci, $p_{adj} = 2 \times 10^{-9}$), and oxidoreductase action (12 loci, $p_{adj} = .05$).

Calcium ion loci include calmodulin, calcineurin, calnexin, calcium-binding proteins in the sarcoplasmic reticulum, and a set of two poorly characterized proteins with calcium-binding motifs (contigs 3436 and 7780). These proteins are EF-hand calcium-binding protein and C-type lectin calcium binding in an hmmer database search (https://www.ebi.ac.uk/Tools/hmmer/). Because calcium ion control is particularly central to calcification in scleractinians, we examined the 77 SNPs from the 13 calcium-related loci for patterns across

populations (Figure 6). As expected, the Grotta Mago population had highly divergent SNP genotypes at these loci (average minor allele frequency difference of 0.24), but these genes also showed a strong degree of linkage among SNP genotypes within a single gene often across 1,000s of base pairs (Figure 6). Such multi-SNP haplotypes are rare in our dataset yet occur in 8 of 10 high excess, calcium ion loci with multiple SNPs.

Given the strong differences in calcium management suggested by excess differentiation of calcium ion genes in Grotta Mago, we queried our transcriptome SNP data base for other genes potentially involved in calcification. In corals, calcification occurs in the calicoblastic space through a combination of high calcium concentration and high pH (reviewed in Drake et al., 2020). High pH is achieved through proton transport by specific calcium/proton pumps, including the plasma membrane calcium ATPase (PMCA). There were no PMCA polymorphisms in our dataset, but the V-type ATPase proton pump (contig DN1551, SNPs 1,701–1,805) showed six of seven SNPs with strong differentiation in Grotta Mago (excess 0.03–28.8,

FIGURE 4 Relationships between age–length growth curves of *Astroides calycularis*. (a) Age–length von Bertalanffy growth curves at the polyp (corallite) level. Dots indicate the age determined by counting the growth bands on computerized tomography. Lines indicate the mean von Bertalanffy growth curve and the 95% confidence interval). Values of L_∞ (maximum expected length in the population) and K (a growth constant, larger for fast growth) were: 7.6 mm and 0.5 for Vent deep; 11.0 mm and 0.2 for Vent shallow; 10.2 mm and 0.2 for Ambient 1; and 11.8 mm and 0.17 for Ambient 2, respectively. (b) Surface 3D rendering of the CT scans performed on a colony of *A. calycularis* from Ambient 1 (A1) and on another colony of similar surface area from Vent deep (Vd). Photograph of the deep vent (Vd) colony shows that same calcification is allocated to a minor number of polyps, and these few polyps result in having a more dense skeleton. (c) Computerized tomography scan to count the growth bands on a single corallite. In this photograph, the corallite of *A. calycularis* is 6 years old; h indicates high-density annual bands

(a)

Grotta Mago (V), deep vent
N = 57; Max Obs. length 7.5 mm

Grotta Mago (V), shallow vent
N = 70; Max Obs. length 10.90 mm

Punta Vico (A1), ambient pH
N = 49; Max Obs. length 10.10 mm

Sant'Angelo (A2), ambient pH
N = 57; Max Obs. length 11.60 mm

Polyp length (mm)

Age (years)
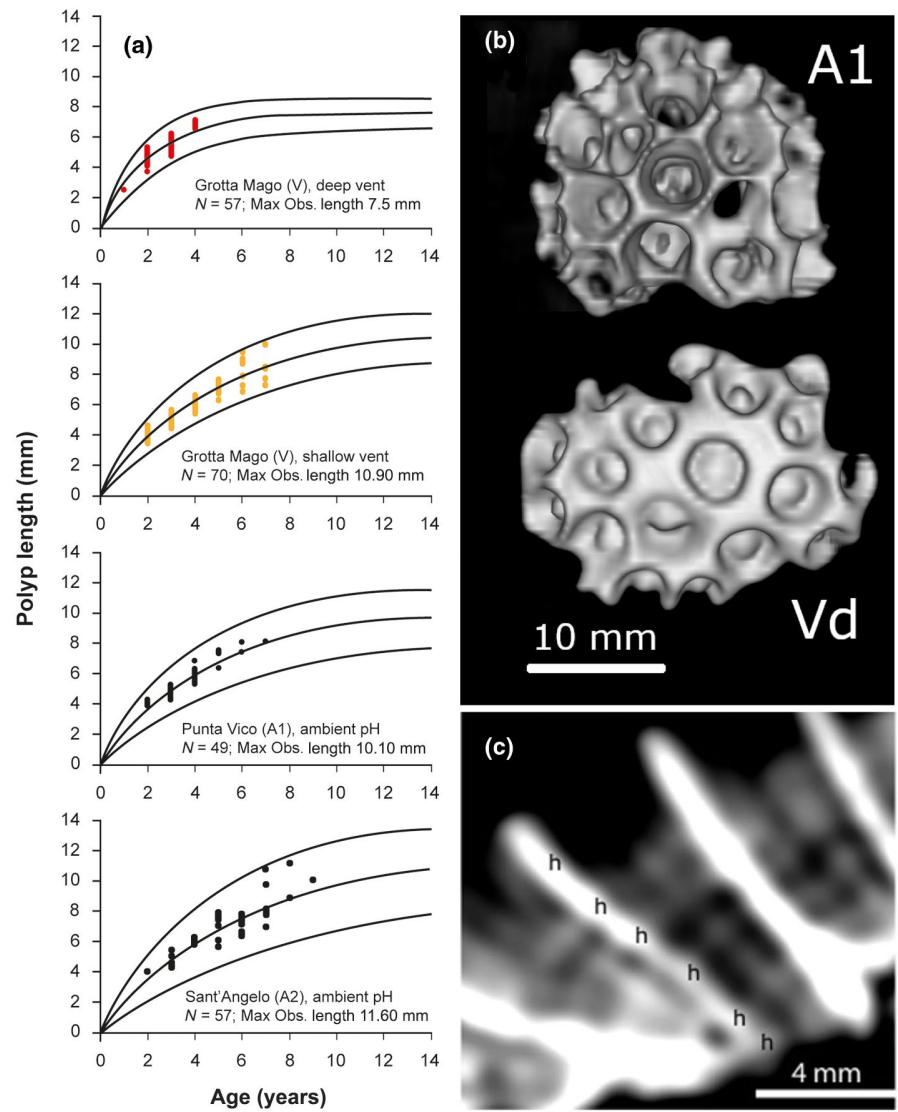
FIGURE 5 Population genetic structure of *Astroides calycularis* based on 46,784 single nucleotide polymorphisms. Number of individuals: CO_2 vent site (Vent, Grotta Mago) = 19; ambient pH sites: Ambient 1 (A1, Punta Vico) = 14, Ambient 2 (A2, Sant'Angelo) = 8

Grotta Mago, Vent
Punta Vico, A1
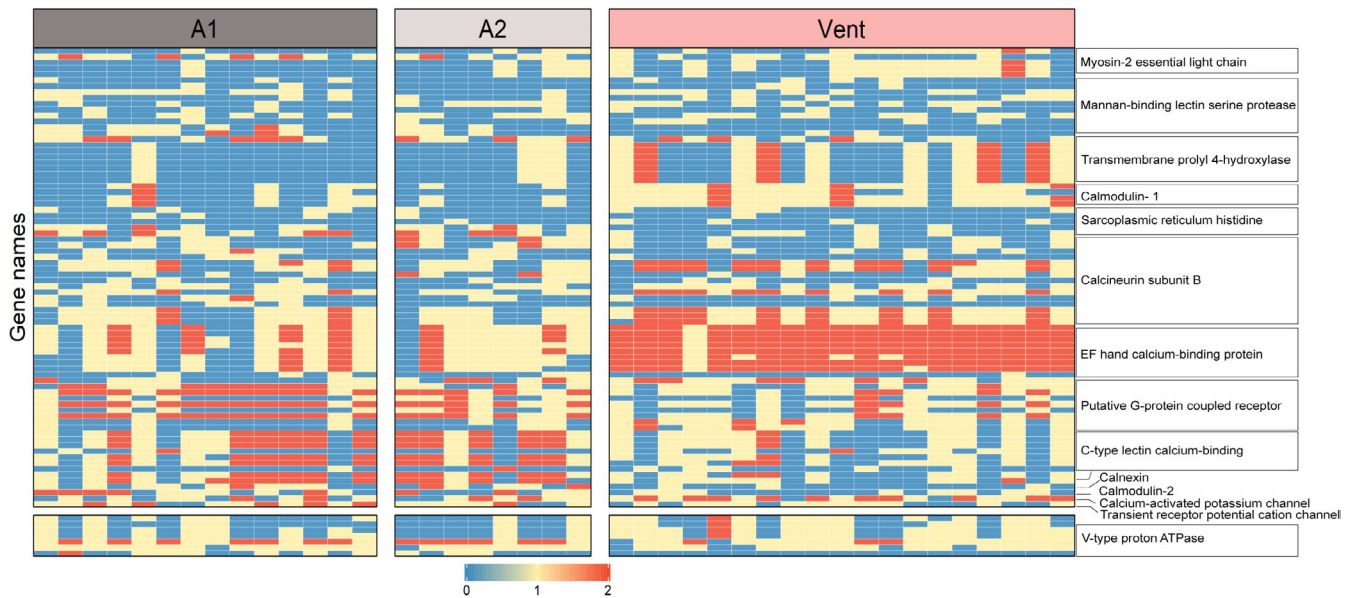Sant'Angelo, A2

PC2

PC1
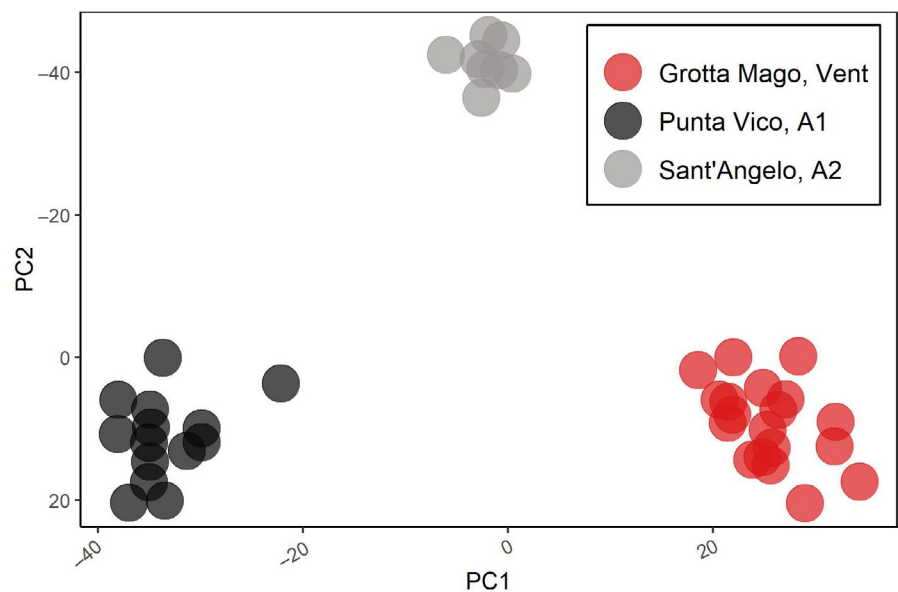
FIGURE 6 Upper: Single nucleotide polymorphism (SNP) genotypes for 13 calcium ion related loci showing high levels of divergence in the Grotta Mago population. Lower: Genotypes for seven SNPs within a highly differentiated V-type proton ATPase potentially involved in pH regulation in the calicoblastic layer where calcification occurs. Vent: CO_2 vent (Grotta Mago), A1: Ambient 1 (Punta Vico); A2: Ambient 2 (Sant'Angelo). 0 = homozygous major allele, 1 = heterozygous; 2 = homozygous minor allele

average 11.4, Figure 6). Minor allele frequencies differed by about a factor of 2 in Grotta Mago compared to the other locations, and SNPs show strong linkage.

In addition to genes involved in calcium and pH regulation, we explored possible adaptation in genes managing intracellular carbonate chemistry. Coral calcification depends on the delivery of CO_2 to the calicoblastic layer where it is converted to carbonate ions (Cohen & McConnaughey, 2003). In *A. calycularis*, a plethora of carbonate-related genes showed high differentiation and high linkage in Grotta Mago, including carboxylases and transporters, but the most interesting is a carbonic anhydrase (contig 15508, 5 of 12 SNPs with excess F_{ST} above 10, average = 10.3). Carbonic anhydrases convert highly diffusive CO_2 into charged carbonate ions, localizing them in the calicoblastic layer and regulating calcification (Chen et al., 2018), though they also play a role in pH regulation of non-calcifying coral cells (Bertucci et al., 2013).

4 | DISCUSSION

This study contributes to increasing our understanding of how coral populations persist under naturally high pCO_2 environments—and therefore how they might cope under future ocean acidification scenarios—and links trait-shifts with local variation in environmental parameters found in this new CO_2 vent system. Our results expand upon previous research on populations of corals exposed to naturally elevated pCO_2 (Crook et al., 2013; Enochs et al., 2015; Fabricius et al., 2011; Fantazzini et al., 2015), demonstrating unexpected shifts in patterns of skeleton and growth of the azooxanthellate coral *A. calycularis*. Specifically, colonies shift to a skeletal phenotype characterized by encrusting morphology,

smaller size, reduced coenosarc tissue, fewer polyps, and less porous and denser skeletons at low pH. However, while individual polyps calcified more (greater net calcification rates), calcification rate of whole colonies were similar across sites. The resulting colony skeletons showed equal linear extension at low and ambient pH conditions, while their polyp skeletons extended faster in acidified conditions (Figure 7). Transcriptomic data revealed strong genetic differentiation among local populations of this low-dispersal species. We found excess differentiation in the Grotta Mago population for genes central to calcification, including genes for calcium management (calmodulin, calcium-binding proteins), pH regulation (V-type proton ATPase), and carbonate localization (carbonic anhydrase).

4.1 | Environmental variability in the CO_2 vent system

The vent system exhibits high temporal variability in seawater pH due to varying CO_2 venting intensity from the seabed, mixing due to variations in stratification, and fundamental thermodynamics processes fundamental to the carbonate system (Takeshita et al., 2015). The carbonate chemistry and in situ monitoring of seawater pH delineated a pH gradient (from 4 to 2 m depth) caused by the distance from the venting. This acidification gradient is important for the colonies exposed to more (deep) or less (shallow) acidified conditions, as reflected by the biological response of *Astroides*. The conditions in these zones are comparable with IPCC projections for near future acidification scenarios (RCP2.6 and RCP8.5), which project a decrease in surface pH from −0.14 to −0.4 pH units by 2100 relative to 1870 (Gattuso et al., 2015). pH and its variability found in this study

FIGURE 7 Schematic summary of the responses on skeletal and growth parameters to ocean acidification measured in the coral *Astroides calycularis* at the polyp and colony levels
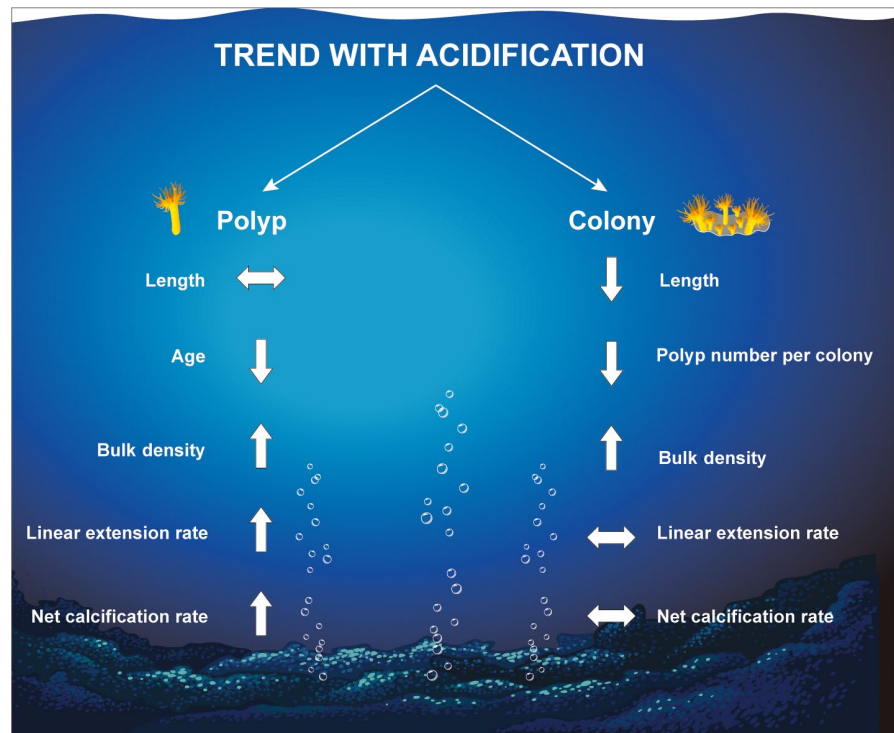
are comparable with the range of natural variation observed in other CO_2 vent systems, with fluctuations of 0.6, 0.7, and 0.5 pH units in coral reefs (Agostini et al., 2018), temperate reefs in Panarea (Prada et al., 2017), and in other CO_2 vents in Ischia (Teixidó et al., 2018), respectively. Likewise, Hofmann et al. (2011) reported pH fluctuations between 0.024 and 1.430 pH units, in which pH measurements were taken from different locations, ranging from polar to tropical, and open-ocean to coastal areas. Interestingly, as mean pH was reduced, its variability and the percentage of pH_T measurements registered below 7.8 units increased, when seawater was uniformly warm. In contrast, in June when the water column was stratified, pH and its variability near the bottom was similar to what was observed in September, whereas, farther from the bottom, pH was higher and less variable. These results indicate that seawater stratification may play a key role in controlling the temporal and depth patterns of pH/pCO_2.

4.2 | Shifts in coral skeleton, growth, and coenosarc

Each scleractinian coral species may adopt different growth strategies in response to ocean acidification. For example, investing calcification resources in bulk skeletal density by sacrificing the rate of linear extension has been observed in *Orbicella annularis* (Carricart-Gavinet, 2007). In contrast, investing calcification resources in linear extension rate at the expense of bulk density has been reported for some *Porites* (Lough & Barnes, 2000) and Dendrophyllidae species (Goffredo et al., 2009). Both strategies may imply different ecological trade-offs for the coral: investing in a denser skeleton results in greater resistance to mechanical stress, while increasing linear extension rate may be advantageous for space competition

and earlier sexual maturity (Goffredo et al., 2009). Unexpectedly, *A. calycularis* revealed unusual patterns in the calcification response to ocean acidification, such as higher bulk skeletal density and lower porosity while maintaining colony linear extension rates and net calcification. This response is different to what was previously shown in solitary corals (e.g., *Balanophyllia europaea*) growing in natural low pH conditions, where a decrease in net calcification resulted from preserving linear extension (to reach the polyp size of sexual maturity) at the expenses of lower bulk density (e.g., increased in skeletal porosity resulting in more fragile skeletons; Fantazzini et al., 2015). Tambutté et al. (2015) found the same response of decreasing calcification and bulk skeletal density while linear extension of skeleton remained unchanged in the tropical coral *Stylophora pistillata* subjected to low pH conditions in laboratory. Mollica et al. (2018) modeled the skeletal growth to changes in seawater chemistry and predicted declines in *Porites* skeletal density but no linear extension across global reefs, reflecting the large variability in the response of coral calcification to ocean acidification. The authors suggested that under low-pH conditions, the increase in linear extension reflects the elongation of calcium carbonate crystals at the site of calcification while the increase in skeletal density reflects the lateral thickening of calcified elements of coral skeleton (Mollica et al., 2018). The unusual response of *A. calycularis* to acidification may reflect an overall maintenance of energetic resources allocated to calcification at the level of the colonies, which extended at the same rate but were composed by fewer polyps, thus partitioning the available energy for calcification among fewer polyps (Swain et al., 2018). We can therefore reasonably assume that nutrients levels, and potentially the zooplankton, did not differ among study sites (Table S2). As a result, a single polyp would have more energetic resources available for calcification than in ambient pH conditions,

as indicated by their greater skeletal growth parameters. This particular response may be possible in *A. calycularis* due to its colonial nature. We hypothesize that to maintain the calcification rate at the colony level, colonies tend to decrease their number of polyps, but in turn, their few polyps extend their skeleton faster to reach the size of sexual maturity. No asexual division (fragmentation) has been observed over 5 years in *A. calycularis* in the three study sites, suggesting that this strategy of reproduction is not common. *A. calycularis* exhibited at the vent site a morphological shift to encrusting and smaller colonies, with less porous, and potentially more robust corallite skeletal architecture.

While individuals from the vents were composed of corallites with higher skeletal density, this was less evident at the colony level. While skeletal integrity was not strictly quantified, observations at the vent site showed that the colonies were more fragile and lost their integrity more readily, suggesting that the section of the skeleton located between the polyps (coenosteum) was either less calcified and/or more prone to dissolution. This could be the result of thinner or absent coenosarc (the tissue covering the coenosteum) found in the colonies at the CO_2 vent. Contrasting responses between skeletal parts that either are or are not protected by living tissues has already been reported for corals (Hennige et al., 2015; Ries J., 2011; Ries J.B., 2011; Rodolfo-Metalpa et al., 2011). This loss of coenosarc could indicate the beginning of a further shift from colonial forms toward solitary polyps to ensure survivorship, as has occurred throughout the history of scleractinian coral evolution and in laboratory conditions (Fine & Tchernov, 2007; Kvitt et al., 2015). Interestingly, it was recently shown that following a heatwave and a bleaching event, the Mediterranean coral *Cladocora caespitosa* suffered from apparent mortality but its tissues actually retracted inside the individual corallites before rejuvenescence occurred a few years later (Kersting & Linares, 2019). Here, we hypothesize that a similar, but less extreme phenomenon occurred with the corals reducing their coenosarc in response to low pH. A reduction in tissue thickness can have implications for calcification because the precipitation of calcium carbonate occurs in the calcifying fluid that is a medium semi-isolated from the external seawater by the overlying coral tissues. To promote calcification, corals have the ability to upregulate pH and C_T (dissolved inorganic carbon) concentrations in the calcifying fluid (Comeau et al., 2017), a capacity that is reduced under ocean acidification (McCulloch et al., 2012). Here reduced calcification between the polyps was likely due to a reduction of coral ability to maintain optimal carbonate chemistry conditions in the calcifying fluid between the polyps. This could have been the result of natural spatial heterogeneity sensitivity of colonies to acidification (Holcomb et al., 2014). In addition to reduced calcification, thinning or disappearing of the tissues likely led to local dissolution because exposed skeletons are more prone to dissolution (Ries J., 2011; Ries J.B., 2011). As a result of reduced calcification and dissolution of the coenosteum, colonies at the vent site were weaker and smaller despite heavily calcified corallites.

4.3 | Genomics of differentiation of corals at the CO_2 vent system

Our results show strong genetic differentiation of all three *A. calycularis* populations (F_{ST} averaging 0.024–0.034), with over 5,000 SNPs showing $F_{ST} > 0.10$. A previous genetic study of *A. calycularis* using microsatellites also found significant genetic differentiation at km-scale distances, likely a reflection of this species limited dispersal capabilities (Casado-Amezúa et al., 2012). These data showed strong linkage among SNPs across 1,000s of bp within genes and strong linkage across different genes. These patterns could be generated by selective sweeps acting on a small number of founder colonies, but because linkage among genes and SNPs occurs among ambient pH (Ambient 1 and Ambient 2) individuals as well as Vent corals. These linkages were probably not due to recent selection at the CO_2 vent site alone but reflect the underlying architecture of adaptation. *A. calycularis* is a warm-water coral whose distribution range is currently expanding northward (Bianchi, 2007), where Ischia belongs to the north-east margin of the confirmed distribution. As a result, it is also likely that selection is acting at the Ambient 1 and 2 sites compared to more southerly populations. Disentangling the ways in which selection at high CO_2 locations combines with selection at higher temperatures may be particularly important in future ocean conditions. The matrix of genetically distinct populations of *A. calycularis* experiencing a variety of selection regimes for heat and CO_2 may be a powerful setting for this future work.

The most highly differentiated genes in the vent site population, Grotta Mago, are annotated for calcium regulation, proton pumping, and inorganic carbon regulation. It is possible that they are differentiated in Grotta Mago for reasons other than selection on calcification in the presence of high CO_2. However, the strong shift in alleles at these loci and the linkage among those differentiated SNPs provides a strong set of hypotheses for the way selection might act to favor coral calcification at low pH.

Two loci of calmodulin were highly differentiated in Grotta Mago, with linked SNPs in our dataset. Calcium transporter genes are thought to be important in delivering calcium to the calicoblastic space (Allemand et al., 2011). Though the precise mechanism is not known, calmodulin along with calbindin and calreticulin are hypothesized to play a role in managing calcium levels and can be sensitive to pH (Allemand et al., 2011). For example, Kaniewska et al. (2012) showed eightfold downregulation of calmodulin in a CO_2-treated reef building coral. An increase in calcium at the site of calcification has been shown as a mean to alleviate the negative effect of low pH in some corals (Decarlo et al., 2018). Our data also showed excess differentiation in genes that depend on calcium concentrations for their function, such as calineurin, calnexin, and the sarcoplasmic reticulum histidine-rich calcium-binding protein, which are thought to play a role in calcium homeostasis.

Intracellular and vacuolar H+ concentrations are central to coral calcification because they can affect pH of the calcifying fluid. The V-type ATPase proton pump is localized in the symbiosomes of corals that contain intracellular symbionts (Tresguerres, 2016), but is also highly expressed in non-symbiotic gastroderm of symbiont-free tips of quickly calcifying corals, suggesting a role in calcification in the absence of symbionts (Perez, 2015). The population of *A. calycularis* in Grotta Mago showed strong differentiation at six SNPs across a 100 bp region of this gene and might reflect a change to acid/base regulation at the vent site.

CO_2 diffuses very quickly through cells, and is hard to localize in cell regions that need it for photosynthesis or calcification. Carbonic anhydrase catalyzes the reaction to convert CO_2 to bicarbonate ions that diffuse much less quickly. In corals, carbonic anhydrase, among other functions, is thought to favor carbonate ion concentration in the calcifying fluid (Chen et al., 2018; Zoccola et al., 2016). It has been hypothesized that increasing carbonic anhydrase activity could be a mean for calcifying organisms to buffer the effects of reduced pH (Zoccola et al., 2016). However, datasets on the importance of carbonic anhydrase are inconsistent: low-pH experiments on a deep water coral (*Lophelia pertusa*) did not find strong shifts in carbonic anhydrase activity, nor did an examination of carbonic anhydrase in polychaete worms from the Ischia CO_2 vents (Del Pasqua et al., 2019). Experiments on reef building corals have shown mixed results (Kurihara et al., 2018). We found strong differentiation of one carbonic anhydrase locus in Grotta Mago. An average shift in minor allele frequency from 0.14 to 0.50 in six linked SNPs may signal differential activity of this gene in some functionally important way. These SNPs appear to be downstream of the carbonic anhydrase coding region and if they play a role it may be as allele-specific regulators of expression. These allele differences may be a good tool to understand the role of carbonic anhydrase in reaction to high CO_2.

In conclusion, our study demonstrates that the natural population of the azooxanthellate coral *A. calycularis* living near the CO_2 vent system shows variable responses in terms of skeleton and growth patterns that result in a shift in phenotypic and ecological traits. We have shown that these variable responses at the polyp and colony level allow this coral to cope with low and variable pH in the long term by re-allocating energy investments between individual and colony growth as well as mineralogical characteristics. Transcriptomic data revealed strong genetic differentiation among local populations with several candidate loci and linkage blocks under selection. In addition, we found excess differentiation in the CO_2 vent population for genes central to calcification, including genes for calcium management (calmodulin, calcium-binding proteins), pH regulation (V-type proton ATPase), and inorganic carbon regulation (carbonic anhydrase). These patterns highlight both the CO_2 vents and the fringes of this species' expansion as potential drivers of adaptation.

CONFLICT OF INTEREST

The authors declare that they have no competing interests.

AUTHOR CONTRIBUTION

N.T., E.C., S.R.P., E.S., S.G., and M.C.G. designed the study. N.T., E.C., S.A., S.C., F.M., A.M., M.M., S.R.P., E.S., L.U., C.D.V., and M.C.G. were involved with fieldwork. N.T., S.A., J.P.G., A.M., S.G.M., L.U., and C.D.V. analyzed the environmental data; E.C., C.C., P.F., and S.G. analyzed the skeletal data; E.S., S.R.P., and N.T. analyzed the genomic data. N.T. drafted the initial manuscript and all authors contributed discussion, writing, and interpretation.

ETHICAL STATEMENT

All work undertaken in this study complied with current laws of Italy and United States of America for collecting and importing/exporting coral specimens. Cites permits IT/EX/2018/MCE/00170, IT/EX/2017/MCE/00214, and IT/EX/2017/MCE/00325.

DATA AVAILABILITY STATEMENT

RNASeq FASTQ files for all 41 samples sequenced in this study were deposited in the NCBI Short Read Archive (SRA) under BioProject PRJNA643775 (accession numbers SRR12135922 and SRR12135962), https://dataview.ncbi.nlm.nih.gov/object/PRJNA643775?reviewer=5j14na61906tr4dne0bvg9kbhq. The de novo transcriptome assembly generated in this study and used for mapping the samples has been deposited in the NCBI Transcriptome Shotgun Assembly (TSA) database at DDBJ/ENA/GenBank under accession number GIRZ01000000 (https://www.ncbi.nlm.nih.gov/nuccore/GIRZ00000000). The version described in this paper is the first version, GIRZ01000000. The bioinformatics scripts used for assembly, mapping, and SNP-calling are available on Github at https://zenodo.org/record/3934433#.X3x00u2xVPY.

ORCID

Núria Teixidó https://orcid.org/0000-0001-9286-2852
Erik Caroselli https://orcid.org/0000-0001-6434-5663
Steeve Comeau https://orcid.org/0000-0002-6724-5286
Jean-Pierre Gattuso https://orcid.org/0000-0002-4533-4114
Fiorenza Micheli https://orcid.org/0000-0002-6865-1438
Alice Mirasole https://orcid.org/0000-0003-2517-9548
Marco Munari https://orcid.org/0000-0002-2702-5393
Elizabeth Sheets https://orcid.org/0000-0002-6335-4952
Lidia Urbini https://orcid.org/0000-0001-7151-7574
Cinzia De Vittor https://orcid.org/0000-0001-8552-4396
Stefano Goffredo https://orcid.org/0000-0002-5022-9503
Maria Cristina Gambi https://orcid.org/0000-0002-0168-776X

REFERENCES

Agostini, S., Harvey, B. P., Wada, S., Kon, K., Milazzo, M., Inaba, K., & Hall-Spencer, J. M. (2018). Ocean acidification drives community shifts towards simplified non-calcified habitats in a subtropical–temperate transition zone. *Scientific Reports*, 8, 11354. https://doi.org/10.1038/s41598-018-29251-7

Allemand, D., Tambutté, É., Zoccola, D., & Tambutté, S. (2011). Coral calcification, cells to reefs. In Z. Dubinsky & N. Stambler (Eds.), *Coral reefs: An ecosystem in transition* (pp. 1–552). Springer.

Bennett, S., Duarte, C. M., Marba, N., & Wernberg, T. (2019). Integrating within-species variation in thermal physiology into climate change ecology. *Philosophical Transactions of the Royal Society B*, 374, 20180550. https://doi.org/10.1098/rstb.2018.0550

Bertucci, A., Moya, A., Tambutté, S., Allemand, D., Supuran, C. T., & Zoccola, D. (2013). Carbonic anhydrases in anthozoan corals – A review. *Bioorganic and Medicinal Chemistry*, 21(6), 1437–1450. https://doi.org/10.1016/j.bmc.2012.10.024

Bianchi, C. N. (2007). Biodiversity issues for the forthcoming tropical Mediterranean Sea. *Hydrobiologia*, 580, 7–21. https://doi.org/10.1007/s10750-006-0469-5

Bozinovic, F., Calosi, P., & Spicer, J. I. (2011). Physiological correlates of geographic range in animals. *Annual Review of Ecology, Evolution, and Systematics*, 42, 155–179. https://doi.org/10.1146/annurev-ecolsys-102710-145055

Brandl, S. J., Rasher, D. B., Côté, I. M., Casey, J. M., Darling, E. S., Lefcheck, J. S., & Duffy, J. E. (2019). Coral reef ecosystem functioning: Eight core processes and the role of biodiversity. *Frontiers in Ecology and the Environment*, 17, 445–454. https://doi.org/10.1002/fee.2088

Camp, E. F., Schoepf, V., Mumby, P. J., Hardtke, L. A., Rodolfo-Metalpa, R., Smith, D. J., & Suggett, D. J. (2018). The future of coral reefs subject to rapid climate change: Lessons from natural extreme environments. *Frontiers in Marine Science*, 5, 4. https://doi.org/10.3389/fmars.2018.00004

Carricart-Gavinet, J. P. (2007). Annual density banding in massive coral skeletons: Result of growth strategies to inhabit reefs with high microborers' activity? *Marine Biology*, 153, 1–5. https://doi.org/10.1007/s00227-007-0780-3

Casado-Amezúa, P., Goffredo, S., Templado, J., & Machordom, A. (2012). Genetic assessment of population structure and connectivity in the threatened Mediterranean coral *Astroides calycularis* (Scleractinia, Dendrophylliidae) at different spatial scales. *Molecular Ecology*, 21, 3671–3685. https://doi.org/10.1111/j.1365-294X.2012.05655.x

Chan, N. C. S., & Connolly, S. R. (2013). Sensitivity of coral calcification to ocean acidification: A meta-analysis. *Global Change Biology*, 19(1), 282–290. https://doi.org/10.1111/gcb.12011

Chen, S., Gagnon, A. C., & Adkins, J. F. (2018). Carbonic anhydrase, coral calcification and a new model of stable isotope vital effects. *Geochimica et Cosmochimica Acta*, 236, 179–197. https://doi.org/10.1016/j.gca.2018.02.032

Cinelli, F., Fresi, E., Mazzella, L., Pansini, M., Pronzato, R., & Svoboda, A. (1977). Distribution of benthic phyto- and zoocoenoses along a light gradient in a superficial marine cave. In B. F. Keegan, P. O. O'Ceidig, & P. J. Boaden (Eds.), *Biology of benthic organisms* (pp. 173–183). Pergamon Press.

Cohen, A. L., & McConnaughey, T. A. (2003). Geochemical perspectives on coral mineralization. In P. M. Dove, S. Weiner, & J. J. DeYoreo (Eds.), *Biomineralization* (Vol. 54, pp. 151–187). The Mineralogical Society of America.

Comeau, S., Cornwall, C. E., & Mcculloch, M. T. (2017). Decoupling between the response of coral calcifying fluid pH and calcification to ocean acidification. *Scientific Reports*, 7, 7573. https://doi.org/10.1038/s41598-017-08003-z

Crook, E. D., Cohen, A. L., Rebolledo-Vieyra, M., Hernandez, L., & Paytan, A. (2013). Reduced calcification and lack of acclimatization by coral colonies growing in areas of persistent natural acidification. *Proceedings of the National Academy of Sciences of the United States of America*, 110(27), 11044–11049. https://doi.org/10.1073/pnas.1301589110

Dappiano, M., & Gambi, M. C. (2004). New data on occurrence of thermophile Scleractinia (Cnidaria, Anthozoa) in the Phlaegrean Island (Ischia, Procida, Vivara, Gulf of Naples), with special attention to *Astroides calycularis*. *Biogeographia – The Journal of Integrative Biogeography*, 25, 1–15. https://doi.org/10.21426/B6110042

Darling, E. S., Alvarez-Filip, L., Oliver, T. A., Mcclanahan, T. R., & Côté, I. M. (2012). Evaluating life-history strategies of reef corals from species traits. *Ecology Letters*, 15(12), 1378–1386. https://doi.org/10.1111/j.1461-0248.2012.01861.x

Decarlo, T. M., Comeau, S., Cornwall, C. E., & McCulloch, M. T. (2018). Coral resistance to ocean acidification linked to increased calcium at the site of calcification. *Proceedings of the Royal Society B: Biological Sciences*, 285(1878), 20180564. https://doi.org/10.1098/rspb.2018.0564

Del Pasqua, M., Gambi, M. C., Caricato, R., Lionetto, M. G., & Giangrande, A. (2019). Effects of short-term and long-term exposure to ocean acidification on carbonic anhydrase activity and morphometric characteristics in the invasive polychaete *Branchiomma boholense* (Annelida: Sabellidae): A case-study from a CO_2 vent system. *Marine Environmental Research*, 144, 203–212. https://doi.org/10.1016/j.marenvres.2019.01.011

Doney, S. C., Fabry, V. J., Feely, R. A., & Kleypas, J. A. (2009). Ocean acidification: The other CO_2 problem. *Annual Review of Marine Science*, 1(1), 169–192. https://doi.org/10.1146/annurev.marine.010908.163834

Drake, J. L., Mass, T., Stolarski, J., Von Euw, S., van de Schootbrugge, B., & Falkowski, P. G. (2020). How corals made rocks through the ages. *Global Change Biology*, 26(1), 31–53. https://doi.org/10.1111/gcb.14912

Enochs, I. C., Manzello, D. P., Donham, E. M., Kolodziej, G., Okano, R., Johnston, L., Young, C., Iguel, J., Edwards, C. B., Fox, M. D., Valentino, L., Johnson, S., Benavente, D., Clark, S. J., Carlton, R., Burton, T., Eynaud, Y., & Price, N. N. (2015). Shift from coral to macroalgae dominance on a volcanically acidified reef. *Nature Climate Change*, 5, 1083–1088. https://doi.org/10.1038/nclimate2758

Fabricius, K. E., Langdon, C., Uthicke, S., Humphrey, C., Noonan, S., De'ath, G., Okazaki, R., Muehllehner, N., Glas, M. S., & Lough, J. M. (2011). Losers and winners in coral reefs acclimatized to elevated carbon dioxide concentrations. *Nature Climate Change*, 1(6), 165–169. https://doi.org/10.1038/NCLIMATE1122

Fantazzini, P., Mengoli, S., Pasquini, L., Bortolotti, V., Brizi, L., Mariani, M., Di Giosia, M., Fermani, S., Capaccioni, B., Caroselli, E., Prada, F., Zaccanti, F., Levy, O., Dubinsky, Z., Kaandorp, J. A., Konglerd, P., Hammel, J. U., Dauphin, Y., Cuif, J.-P., … Goffredo, S. (2015). Gains and losses of coral skeletal porosity changes with ocean acidification acclimation. *Nature Communications*, 6, 7785. https://doi.org/10.1038/ncomms8785

Fine, M., & Tchernov, D. (2007). Scleractinian coral species survive and recover from decalcification. *Science*, 315(5820), 1811. https://doi.org/10.1126/science.1137094

Gattuso, J.-P., Magnan, A., Bille, R., Cheung, W. W. L., Howes, E. L., Joos, F., Allemand, D., Bopp, L., Cooley, S. R., Eakin, C. M., Hoegh-Guldberg, O., Kelly, R. P., Pörtner, H.-O., Rogers, A. D., Baxter, J. M., Laffoley, D., Osborn, D., Rankovic, A., Rochette, J., … Turley, C. (2015). Contrasting futures for ocean and society from different anthropogenic CO_2 emissions scenarios. *Science*, 349, aac4722. https://doi.org/10.1126/science.aac4722

Goffredo, S., Caroselli, E., Mattioli, G., Pignotti, E., Dubinsky, Z., & Zaccanti, F. (2009). Inferred level of calcification decreases along

an increasing temperature gradient in a Mediterranean endemic coral. *Limnology and Oceangraphy*, *54*(3), 930–937. https://doi.org/10.4319/lo.2009.54.3.0930

Goffredo, S., Prada, F., Caroselli, E., Capaccioni, B., Zaccanti, F., Pasquini, L., Fantazzini, P., Fermani, S., Reggi, M., Levy, O., Fabricius, K. E., Dubinsky, Z., & Falini, G. (2014). Biomineralization control related to population density under ocean acidification. *Nature Climate Change*, *4*(7), 593–597. https://doi.org/10.1038/NCLIMATE2241

Hall-Spencer, J. M., Rodolfo-Metalpa, R., Martin, S., Ransome, E., Fine, M., Turner, S. M., Rowley, S. J., Tedesco, D., & Buia, M.-C. (2008). Volcanic carbon dioxide vents show ecosystem effects of ocean acidification. *Nature*, *454*(7200), 96–99. https://doi.org/10.1038/nature07051

Hennige, S. J., Wicks, L. C., Kamenos, N. A., Perna, G., Findlay, H. S., & Roberts, J. M. (2015). Hidden impacts of ocean acidification to live and dead coral framework. *Proceeding Royal Society B*, *282*, 20150990. https://doi.org/10.1098/rspb.2015.0990

Hoffmann, A. A., & Sgro, C. M. (2011). Climate change and evolutionary adaptation. *Nature*, *470*, 479–485. https://doi.org/10.1038/nature09670

Hofmann, G. E., Smith, J. E., Johnson, K. S., Send, U., Levin, L. A., Micheli, F., Paytan, A., Price, N. N., Peterson, B., Takeshita, Y., Matson, P. G., Crook, E. D., Kroeker, K. J., Gambi, M. C., Rivest, E. B., Frieder, C. A., Yu, P. C., & Martz, T. R. (2011). High-frequency dynamics of ocean pH: A multi-ecosystem comparison. *PLoS ONE*, *6*(12), e28983. https://doi.org/10.1371/journal.pone.0028983

Holcomb, M., Venn, A. A., Tambutté, E., Tambutté, S., Allemand, D., Trotter, J., & McCulloch, M. (2014). Coral calcifying fluid pH dictates response to ocean acidification. *Scientific Reports*, *4*, 5207. https://doi.org/10.1038/srep05207

Kaniewska, P., Campbell, P. R., Kline, D. I., Rodriguez-Lanetty, M., Miller, D. J., Dove, S., & Hoegh-Guldberg, O. (2012). Major cellular and physiological impacts of ocean acidification on a reef building coral. *PLoS ONE*, *7*(4), e34659. https://doi.org/10.1371/journal.pone.0034659

Kapsenberg, L., & Cyronak, T. (2019). Ocean acidification refugia in variable environments. *Global Change Biology*, *25*(10), 3201–3214. https://doi.org/10.1111/gcb.14730

Kersting, D. K., & Linares, C. (2019). Living evidence of a fossil survival strategy raises hope for warming-affected corals. *Science Advances*, *5*(10), eaax2950. https://doi.org/10.1126/sciadv.aax2950

Kroeker, K. J., Bell, L. E., Donham, E. M., Hoshijima, U., Lummis, S., Toy, J. A., & Norton, E. W. (2019). Ecological change in dynamic environments: Accounting for temporal environmental variability in studies of ocean change biology. *Global Change Biology*, *26*(1), 54–67. https://doi.org/10.1111/gcb.14868

Kurihara, H., Takahashi, A., Reyes-Bermudez, A., & Hidaka, M. (2018). Intraspecific variation in the response of the scleractinian coral *Acropora digitifera* to ocean acidification. *Marine Biology*, *165*(2), 38. https://doi.org/10.1007/s00227-018-3295-1

Kvitt, H., Kramarsky-Winter, E., Maor-Landaw, K., Zandbank, K., Kushmaro, A., Rosenfeld, H., Fine, M., & Tchernov, D. (2015). Breakdown of coral colonial form under reduced pH conditions is initiated in polyps and mediated through apoptosis. *Proceedings of the National Academy of Sciences of the United States of America*, *112*(7), 2082–2086. https://doi.org/10.1073/pnas.1419621112

Lough, J. M., & Barnes, D. J. (2000). Environmental controls on growth of the massive coral Porites. *Journal of Experimental Marine Biology and Ecology*, *245*, 225–243. https://doi.org/10.1016/S0022-0981(99)00168-9

McCulloch, M., Falter, J., Trotter, J., & Montagna, P. (2012). Coral resilience to ocean acidification and global warming through pH up-regulation. *Nature Climate Change*, *2*(8), 623–627. https://doi.org/10.1038/nclimate1473

Mollica, N. R., Guo, W., Cohen, A. L., Huang, K. F., Foster, G. L., Donald, H. K., & Solow, A. R. (2018). Ocean acidification affects coral growth by reducing skeletal density. *Proceedings of the National Academy of Sciences of the United States of America*, *115*(8), 1754–1759. https://doi.org/10.1073/pnas.1712806115

Mouillot, D., Graham, N. A. J., Villéger, S., Mason, N. W. H., & Bellwood, D. R. (2013). A functional approach reveals community responses to disturbances. *Trends in Ecology & Evolution*, *28*(3), 167–177. https://doi.org/10.1016/j.tree.2012.10.004

Movilla, J., Calvo, E., Coma, R., Serrano, E., López-Sanz, À., & Pelejero, C. (2016). Annual response of two Mediterranean azooxanthellate temperate corals to low-pH and high-temperature conditions. *Marine Biology*, *163*, 135. https://doi.org/10.1007/s00227-016-2908-9

Palumbi, S. R., Barshis, D. J., Traylor-Knowles, N., & Bay, R. A. (2014). Mechanisms of reef coral resistance to future climate change. *Science*, *344*, 895–898. https://doi.org/10.1126/science.1251336

Perez, S. O. (2015). *Characterization of sodium potassium ATPase and vacuolar proton-ATPase in three coral species from two different clades*. Thesis/dissertation, University of California San Diego. Retrieved from https://escholarship.org/uc/item/0xp4r2hb

Prada, F., Caroselli, E., Mengoli, S., Brizi, L., Fantazzini, P., Capaccioni, B., Pasquini, L., Fabricius, K. E., Dubinsky, Z., Falini, G., & Goffredo, S. (2017). Ocean warming and acidification synergistically increase coral mortality. *Scientific Reports*, *7*, 40842. https://doi.org/10.1038/srep40842

Ries, J. (2011). Acid ocean cover up. *Nature Climate Change*, *1*, 294–295. https://doi.org/10.1038/nclimate1204

Ries, J. B. (2011). A physicochemical framework for interpreting the biological calcification response to CO_2-induced ocean acidification. *Geochimica et Cosmochimica Acta*, *75*(14), 4053–4064. https://doi.org/10.1016/j.gca.2011.04.025

Rodolfo-Metalpa, R., Houlbrèque, F., Tambutté, É., Boisson, F., Baggini, C., Patti, F. P., Jeffree, R., Fine, M., Foggo, A., Gattuso, J.-P., & Hall-Spencer, J. M. (2011). Coral and mollusc resistance to ocean acidification adversely affected by warming. *Nature Climate Change*, *1*(9), 1–5. https://doi.org/10.1038/nclimate1200

Savolainen, O., Lascoux, M., & Merilä, J. (2013). Ecological genomics of local adaptation. *Nature Reviews Genetics*, *14*(11), 807–820. https://doi.org/10.1038/nrg3522

Swain, T. D., Bold, E. C., Osborn, P. C., Baird, A. H., Westneat, M. W., Backman, V., & Marcelino, L. A. (2018). Physiological integration of coral colonies is correlated with bleaching resistance. *Marine Ecology Progress Series*, *586*, 1–10. https://doi.org/10.3354/meps12445

Takeshita, Y., Frieder, C. A., Martz, T. R., Ballard, J. R., Feely, R. A., Kram, S., Nam, S., Navarro, M. O., Price, N. N., & Smith, J. E. (2015). Including high frequency variability in coastal ocean acidification projections. *Biogeosciences*, *12*(9), 7125–7176. https://doi.org/10.5194/bgd-12-7125-2015

Tambutté, E., Venn, A. A., Holcomb, M., Segonds, N., Techer, N., Zoccola, D., Allemand, D., & Tambutté, S. (2015). Morphological plasticity of the coral skeleton under CO_2-driven seawater acidification. *Nature Communications*, *6*(7368), 1–9. https://doi.org/10.1038/ncomms8368

Teixidó, N., Gambi, M. C., Parravicini, V., Kroeker, K., Micheli, F., Villéger, S., & Ballesteros, E. (2018). Functional biodiversity loss along natural CO_2 gradients. *Nature Communications*, *9*, 5149. https://doi.org/10.1038/s41467-018-07592-1

Thomas, L., Rose, N. H., Bay, R. A., López, E. H., Morikawa, M. K., Ruiz-Jones, L., & Palumbi, S. R. (2018). Mechanisms of thermal tolerance in reef-building corals across a fine-grained environmental mosaic: Lessons from Ofu, American Samoa. *Frontiers in Marine Science*, *4*, 434. https://doi.org/10.3389/fmars.2017.00434

Tresguerres, M. (2016). Novel and potential physiological roles of vacuolar-type H$^+$-ATPase in marine organisms. *Journal of Experimental Biology*, *219*(14), 2088–2097. https://doi.org/10.1242/jeb.128389

Turner, J. S. (1973). *Buoyancy effects in fluids*. Cambridge University Press.

Zibrowius, H. (1995). The "southern" *Astroides calycularis* in the Pleistocene of the northern Mediterranean—An indicator of climatic changes (Cnidaria, Scleractinia). *Geobios*, *28*, 9–16. https://doi.org/10.1016/S0016-6995(95)80201-0

Zoccola, D., Innocenti, A., Bertucci, A., Tambutté, E., Supuran, C. T., & Tambutté, S. (2016). Coral carbonic anhydrases: Regulation by ocean acidification. *Marine Drugs*, *14*, 109. https://doi.org/10.3390/md14060109

SUPPORTING INFORMATION

Additional supporting information may be found online in the Supporting Information section.

How to cite this article: Teixidó N, Caroselli E, Alliouane S, et al. Ocean acidification causes variable trait-shifts in a coral species. *Glob Change Biol*. 2020;00:1–18. https://doi.org/10.1111/gcb.15372